

Underlay Radar-Massive MIMO Spectrum Sharing: Modeling Fundamentals and Performance Analysis

RaghuNandan M. Rao, Harpreet S. Dhillon, Vuk Marojevic, and Jeffrey H. Reed

Abstract

In this work, we investigate underlay radar-massive MIMO cellular coexistence in LoS/near-LoS channels, where both systems are capable of 3D beamforming. The cellular base station (BS) locations are modeled using a homogeneous Poisson point process (PPP), and a single radar is located at the center of a circular exclusion zone (EZ) within which the BSs are prohibited from operating. We derive an analytical expression of a tight upper bound on the average interference power at the radar due to the massive MIMO downlink. This calculation is based on a novel construction in which each Poisson Voronoi (PV) cell is bounded by its circumcircle in order to bound the effect of the random cell shapes on average interference. However, this model is intractable for characterizing the interference distribution, due to the correlation between the shapes and sizes of adjacent PV cells. Hence, we propose a tractable nominal interference model, where each PV cell is modeled as a circular disk with area equal to the average area of the typical cell. We quantify the gap in the average interference power between these two models, and show that the upper bound is tight for realistic deployment parameters. Under the nominal interference model, we derive the equal interference contour in closed-form, and characterize the interference distribution using the dominant interferer approximation. Finally, we use tractable expressions for the interference distribution to characterize important radar performance metrics such as the spatial probability of false alarm/detection in a quasi-static target tracking scenario. We validate the accuracy of our analytical approximations using numerical results, which (a) reveal useful trends in the average interference as a function of the deployment parameters (BS density, exclusion zone radius, antenna height, transmit power of each BS etc.), and (b) provide useful system design insights in the form of radar receiver operating characteristic (ROC) curves for current and future radar-cellular spectrum sharing scenarios.

R. M. Rao, H. S. Dhillon and J. H. Reed are with Wireless@VT, Bradley Department of ECE, Virginia Tech, Blacksburg, VA, 24061, USA (e-mail: {raghumr, hdhillon, reedjh}@vt.edu). V. Marojevic is with the Department of ECE at Mississippi State University, Mississippi State, MS, 39762, USA (e-mail: vuk.marojevic@ece.msstate.edu). The support of the U.S. NSF Grants CNS-1564148, CNS-1642873, and ECCS-1731711 is gratefully acknowledged. This work was presented in part at IEEE Globecom, Waikoloa, HI, USA, 2019 [1].

Index Terms

Stochastic geometry, radar-massive MIMO coexistence, interference distribution, probability of false alarm, probability of detection.

I. INTRODUCTION

Over the last few years, wireless networks have evolved across all layers in order to meet the ever-increasing demand for user data. At the physical layer, technologies such as spectrum sharing [2] and massive MIMO [3] have been investigated by academia and the industry to increase the spectral efficiency by an order of magnitude in comparison to the previous generation.

Massive MIMO boosts spectral efficiency by spatially multiplexing multiple users on the same time-frequency resource using large antenna arrays. Pioneering research by industry and academia on the fundamental aspects [3], [4], real-world channel measurements [5], prototyping [6] and standardization [7], has led to the deployment of massive MIMO technologies in the Third Generation Partnership Project (3GPP) Long-Term Evolution-Advanced Pro (LTE-A Pro) and 5G New Radio (NR) wireless networks.

On the other hand, the objective of spectrum sharing schemes is to improve spectral utilization by facilitating the coexistence of multiple wireless technologies and services on the same frequency bands. In the United States, regulatory support through the Federal Communications Commission's (FCC) ratification of spectrum sharing rules for the 3.5 GHz [8] and 5 GHz [9] frequency bands has incentivized network providers to deploy cellular base stations and network infrastructure in these bands. Concurrently, the wireless industry's standardization efforts have led to adapting cellular networks for operating in unlicensed and shared frequency bands through technologies such as License Assisted Access (LAA) [10] and 5G New Radio-Unlicensed (5G NR-U) [11].

Spectrum sharing is particularly attractive in the congested sub-6 GHz frequency bands, where radar systems are the biggest consumer of radio spectrum. Underlay spectrum sharing is a popular method, where the establishment of an exclusion zone limits cellular (secondary user) interference to the radar (primary user) below the desired interference threshold, often in the absence of cooperation between the sharing entities. This radar-cellular coexistence scenario is the topic of the current paper. Due to the lack of coordination between the radar and cellular systems, it is critically important to understand the impact of the worst-case interference seen by the radar systems due to cellular transmissions. Since modern radar and cellular antenna

arrays are capable of 3D beamforming, it is necessary to incorporate it into such analyses. Unfortunately, systematic modeling of 3D beamforming in the study of large-scale spectrum sharing systems is overlooked in the current works. In this paper, we bridge this knowledge gap by (a) methodically incorporating 3D beamforming capabilities of the radar and massive MIMO BSs in our system model, and (b) comprehensively evaluating the impact of worst-case cellular interference on radar performance metrics, as a function of key deployment parameters.

A. *Related Work*

Prior works have considered different approaches for radar-cellular coexistence, which can be broadly classified under:

- Multi-antenna techniques: These leverage the additional spatial degrees of freedom to mitigate mutual interference between the radar and cellular system [12], [13], [14], [15].
- Waveform design: The waveform of the radar [16], [17] and cellular system [18], [19] can be designed to enhance resilience of the receiver to interference.
- Opportunistic spectrum sharing: These schemes improve the secondary system (cellular) performance by exploiting information of the temporal/spectral/spatial variation of primary user interference [20], [21].

Accurate channel state information (CSI) is crucial for multi-antenna techniques to be effective, for which cooperation schemes such as common knowledge of radar and cellular probing waveforms is necessary [22]. However, security concerns make cooperation impossible with military and air traffic control radar systems, which occupy a significant portion of sub-6 GHz bands. Meanwhile, the adoption of interference-resilient waveforms has been very slow, since they require significant modifications to both systems, making their mass deployment infeasible in the near future. While opportunistic spectrum access is feasible in the case of rotating radars in the ‘search mode’ [20], it is not possible for all base stations to operate when the radar is tracking a target. In the absence of cooperation, a static exclusion zone is defined around the radar to limit cellular interference below a predefined threshold.

To accurately analyze the impact of cellular interference on radar performance metrics, it is important to consider a large-scale cellular network. While system-level simulators are often used to study such networks, their high complexity results in very lengthy execution times, and it is difficult to benchmark them and extract fundamental insights. Due to its analytical tractability, stochastic geometry has become a useful tool to analyze large scale behavior of spectrum sharing

scenarios such as LTE-WiFi coexistence [23], [24], [25], radar-WiFi coexistence [26], [27], and cellular-D2D coexistence [28], [29], [30].

In radar-cellular coexistence where both systems are equipped with 3D beamforming capabilities [7], modeling the impact of azimuth as well as elevation beamforming gains are crucial to accurately model the received interference power. However, most of the prior work in stochastic geometry consider uniform linear arrays with *only azimuth beamforming capabilities*, and the beamforming pattern is approximated by a piecewise constant function, often obtained from the main lobe and the two side lobe gains [31], or the exact beamforming pattern [26], [27]. Even though some recent works in stochastic geometry account for the elevation beamforming gain in their analysis, the models aren't well-suited for analytical treatment [32], [33], or focus on fixed downtilt scenarios for optimal coverage in multi-cellular networks [34], [35].

B. Contributions

In this work, we develop a novel and tractable analytical framework to analyze radar performance metrics in a radar-massive MIMO spectrum sharing scenario. We consider a single radar system located at the origin, tracking a target above the horizon using a single beam from a uniform rectangular array (URA). The radar is surrounded by massive MIMO BSs, which are distributed as a homogeneous Poisson point process (PPP). All BSs are equipped with a URA mounted at the same height, where each BS is serving multiple users in its cell using hybrid 3D beamforming [4]. A circular exclusion zone (EZ) is established around the radar, and only the BSs lying outside the EZ are allowed to operate.

Worst-Case Average Interference Power: Massive MIMO BS operations result in the worst-case interference for the radar when they serve edge users located in the general direction of the radar. However, incorporating elevation beamforming into the stochastic geometry framework is challenging, since Voronoi cells of the BSs can be arbitrarily large. To overcome this, we devise a novel formulation based on the circumradius distribution of the Voronoi cell [36], termed as the *Circumcircle-based cell (CBC) model*. In addition, the presence of sidelobes result in a beamforming gain pattern that is a non-monotonic function of the elevation angle. We derive an upper bound on the beamforming gain that monotonically decreases with the elevation angle, which is crucial to deriving the upper bound on the worst-case average interference. To develop a tractable and easy-to-use approximation, we also derive the nominal average interference power by modeling each Voronoi cell as a circle of area equal to the average area of a typical

cell, termed as the *Average Area-Equivalent Circular Cell (AAECC) model*. Finally, we provide approximations, that lead to the development of intuitive system design insights regarding the worst-case exclusion zone radius, scaling laws, and the gap between the worst-case and nominal average interference values.

Interference Distribution: The CBC model is intractable for characterization of the interference distribution, since it induces correlation in the circumradii of adjacent PV cells. Therefore, under the AAECC model, we use the dominant interferer method [25], [37], [38], [39] to derive an approximate but accurate expression for the interference distribution. However, this approach is non-trivial since receive beamforming at the radar URA distorts the radial symmetry of the equi-interference contour, unlike the case of omnidirectional reception where it is a circle [39]. A novel intermediate result is the derivation of the *equal interference contour*, which resembles a 2D slice of the 3D radar beamforming pattern, when the exclusion zone radius is much larger than the BS antenna deployment height. We use this to characterize the total interference distribution in terms of that of the *farthest distance of the contour from the radar*.

Radar Performance Metrics: Under a Gaussian signaling scheme [40], we characterize the radar detection and false alarm probabilities averaged over the BS point process [28] in a quasi-static target scenario. We derive the exact probabilities, and develop accurate approximations using the dominant interferer method and the central limit theorem. Performance trends and tradeoffs are demonstrated using radar receiver operating characteristic (ROC) curves, and system design insights for future radar-massive MIMO spectrum sharing deployments are presented.

II. SYSTEM MODEL

We consider the radar-massive MIMO spectrum sharing scenario shown in Fig. 1a. The radar is the primary user (PU), equipped with a $N_{\text{az}}^{(\text{rad})} \times N_{\text{e1}}^{(\text{rad})}$ uniform rectangular array (URA) with $\frac{\lambda}{2}$ -spacing, mounted at a height of h_{rad} m. The massive MIMO downlink is the secondary user (SU), with each BS serving K users with equal power allocation using multi-user MIMO (MU-MIMO). Each BS is equipped with a $N_{\text{az}}^{(\text{BS})} \times N_{\text{e1}}^{(\text{BS})}$ URA with $\frac{\lambda}{2}$ -spacing, mounted at a height of h_{BS} m. The subscripts az (e1) are used to denote the azimuth (elevation) elements respectively, and superscripts rad (BS) denote the radar (BS) antenna elements respectively. The radar is protected from SU interference by a *circular exclusion zone* of radius r_{exc} . The exclusion zone is chosen to be circular since there is no coordination between the cellular network and

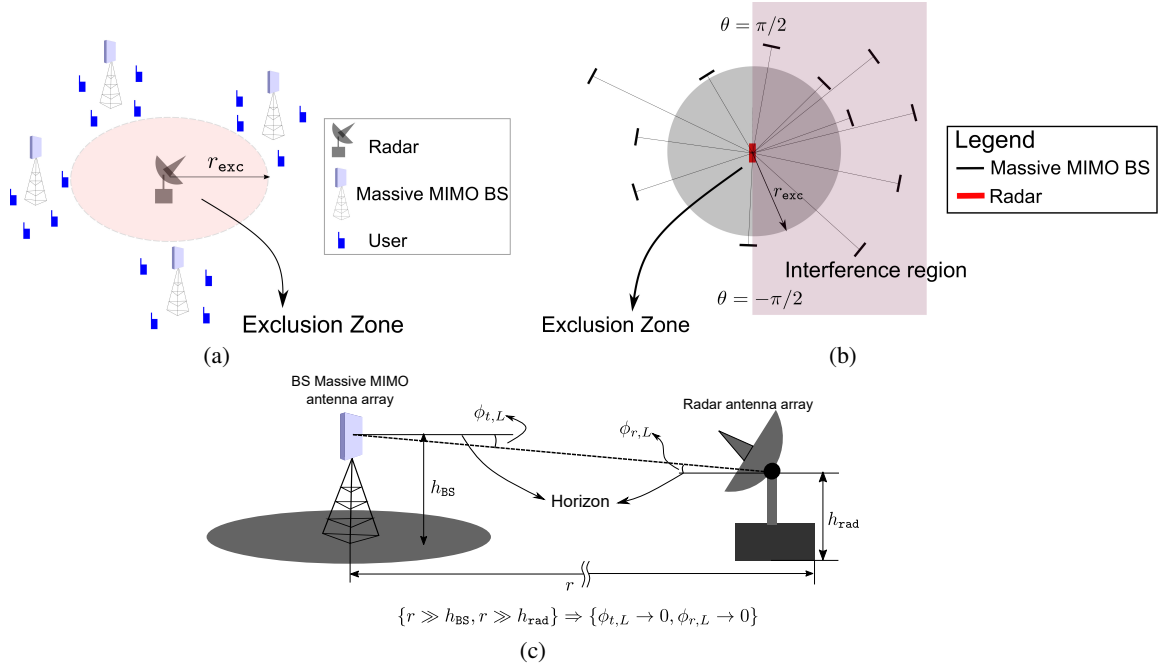


Fig. 1. (a) Illustration of the radar-massive MIMO spectrum sharing scenario. The radar is protected from massive MIMO downlink interference by an exclusion zone of radius r_{exc} . (b) Top View: the boresight of each BS is aligned along the direction of the radar, and the radar receives interference from the azimuth $[-\pi/2, \pi/2]$ depicted by the shaded region. (c) The LoS component has elevation angle of departure ($\theta_{t,L}$) and arrival ($\theta_{r,L}$) close to 0° , i.e. the horizon. In our convention, $-\pi/2 \leq \phi < 0^\circ$ for elevation angles above the horizon, and $0 < \phi \leq \pi/2$ for elevation angles below the horizon.

the radar system, and the radar is assumed to search for a target uniformly at random in the azimuth $[-\frac{\pi}{2}, \frac{\pi}{2}]$, as shown in Fig. 1.

A. Channel Model

In quasi-stationary channel conditions, the spatial channel between each BS and the radar is given by [41]

$$\mathbf{H}_{\mathbf{R}} = \sqrt{\frac{\beta(d)}{1+K_R}} \left(\sqrt{K_R} \mathbf{a}(\theta_{t,L}, \phi_{t,L}) \mathbf{a}^H(\theta_{r,L}, \phi_{r,L}) + \sqrt{\frac{1}{N_c}} \sum_{i=1}^{N_c} \gamma_i \mathbf{a}(\theta_{t,i}, \phi_{t,i}) \mathbf{a}^H(\theta_{r,i}, \phi_{r,i}) \right), \quad (1)$$

where $\beta(d) = PL(r_0)d^{-\alpha}$ is the path loss at distance d , $PL(r_0)$ is the path-loss at reference distance r_0 , α is the path-loss exponent ($\alpha > 2$), d is the 3D distance between the BS and the radar, and N_c is the number of discrete multipath components (MPCs). The Rician factor $K_R \gg 1$, where propagation is dominated by the LoS component¹. In addition, the random

¹Such propagation scenarios are observed in (a) coastal deployments (for e.g., terrestrial BSs sharing spectrum with a naval radar), and (b) terrestrial deployments in flat rural/suburban terrain (for e.g., terrestrial BSs sharing spectrum with a terrestrial radar).

small-scale fading amplitude satisfies $\mathbb{E}[\gamma_i] = 0$ and $\mathbb{E}[|\gamma_i|^2] = 1$. The azimuth and elevation angles of arrival (departure) of the i^{th} MPC at the radar (from the BS) is denoted by $\theta_{r,i}$ ($\theta_{t,i}$) and $\phi_{r,i}$ ($\phi_{t,i}$), respectively. Similarly, the azimuth and elevation angles of departure (arrival) of the LoS component are given by $\theta_{t,L}$ ($\theta_{r,L}$) and $\phi_{t,L}$ ($\phi_{r,L}$), respectively, as shown in Fig. 1c. The steering vector $\mathbf{a}(\theta_t, \phi_t) \in \mathbb{C}^{M_{\text{rad}} \times 1}$ (BS), and $\mathbf{a}(\theta_r, \phi_r) \in \mathbb{C}^{M_{\text{rad}} \times 1}$ (radar) is defined in Appendix A, where $M_{\text{BS}} = N_{\text{az}}^{(\text{BS})} \times N_{\text{el}}^{(\text{BS})}$ and $M_{\text{rad}} = N_{\text{az}}^{(\text{rad})} \times N_{\text{el}}^{(\text{rad})}$.

B. Massive MIMO Downlink Beamforming Model

The massive MIMO downlink serves K users located in clusters with mutually disjoint angular support using joint spatial division multiplexing (JSDM) [4]. We consider a highly spatially correlated downlink channel, given by the one-ring model as $\mathbf{h}_i = \sqrt{\beta_i} \mathbf{U}_i \mathbf{\Lambda}_i^{1/2} \mathbf{z}_i \in \mathbb{C}^{M_{\text{BS}} \times 1}$ [4], where β_i is the large-scale pathloss for the i^{th} user, $\mathbf{U}_i \in \mathbb{C}^{M_{\text{BS}} \times r}$ is the orthonormal matrix of eigenvectors, $\mathbf{\Lambda}_i \in \mathbb{R}^{r \times r}$ is the diagonal matrix of eigenvalues, and $\mathbf{z}_i \sim \mathcal{CN}(\mathbf{0}, \mathbf{I}_r) \in \mathbb{C}^{r \times 1}$ is a complex Gaussian random vector, where $r \ll M_{\text{BS}}$ is the channel rank in the high spatially correlated downlink channel [4]. For simplicity, we consider that all users in the network have the same channel rank. The received signal $\mathbf{y} \in \mathbb{C}^{K \times 1}$ can be written as

$$\mathbf{y} = \mathbf{H}^H \mathbf{W}_{\text{RF}} \mathbf{W}_{\text{BB}} \mathbf{d} + \mathbf{n}, \quad (2)$$

where $\mathbf{W}_{\text{RF}} = [\mathbf{w}_{\text{RF},1} \ \mathbf{w}_{\text{RF},2} \ \cdots \ \mathbf{w}_{\text{RF},K}] \in \mathbb{C}^{M_{\text{BS}} \times K}$ is the RF beamformer that groups user clusters with disjoint angular support using nearly orthogonal beams, and $\mathbf{W}_{\text{BB}} = [\mathbf{w}_{\text{BB},1} \ \cdots \ \mathbf{w}_{\text{BB},K}] \in \mathbb{C}^{K \times K}$ is the baseband precoder [4]. If the azimuth and elevation angular support of the k^{th} user cluster is given by $\Theta_k = [\theta_k^{(\min)}, \theta_k^{(\max)}]$ and $\Phi_k = [\phi_k^{(\min)}, \phi_k^{(\max)}]$, then without loss of generality we consider that the RF beamformer is given by $\mathbf{w}_{\text{RF},k} = \frac{1}{\sqrt{M_{\text{BS}}}} \mathbf{a}(\theta_k, \phi_k)$, where $\theta_k = (\theta_k^{(\min)} + \theta_k^{(\max)})/2$ and $\phi_k = (\phi_k^{(\min)} + \phi_k^{(\max)})/2$. The data $\mathbf{d} = [d_1 \ d_2 \ \cdots \ d_K]^T \in \mathbb{C}^{K \times 1}$, such that $\mathbb{E}[\mathbf{d}] = \mathbf{0}$ and $\mathbb{E}[\mathbf{d}\mathbf{d}^H] = \frac{P_{\text{BS}}}{K} \mathbf{I}$, where d_k is the symbol intended for the k^{th} UE and P_{BS} is the total transmit power per BS. The noise $\mathbf{n} \in \mathbb{C}^{K \times 1}$ is spatially white with $\mathbf{n} \sim \mathcal{CN}(\mathbf{0}, \sigma_n^2 \mathbf{I})$.

Proposition 1. *For the massive MIMO BS in the asymptotic regime, the baseband precoding matrix $\mathbf{W}_{\text{BB}} \approx \mathbf{I}$ for Zero-Forcing (ZF) and Maximum Ratio Transmission (MRT), when K users from different clusters with mutually disjoint angular support are served.*

Proof. (Sketch) The MRT and ZF precoders are $\mathbf{W}_{\text{BB}}^{(\text{MRT})} = \mathbf{W}_{\text{RF}}^H \mathbf{H}$ and $\mathbf{W}_{\text{BB}}^{(\text{ZF})} = (\mathbf{H}^H \mathbf{W}_{\text{RF}})^{-1}$ respectively. In the asymptotic regime $\mathbf{W}_{\text{RF}}^H \mathbf{W}_{\text{RF}} \approx \mathbf{I}$ [4]. For users in clusters with mutually disjoint angular support, $\mathbf{U}_i^H \mathbf{w}_{\text{RF},j} \approx 0, i \neq j$ [4]. Therefore, $\mathbf{H}^H \mathbf{W}_{\text{RF}} \approx \mathbf{\Upsilon} = \text{diag}[v_1 \ v_2 \ \cdots \ v_K]$.

Since $\mathbb{E}[\mathbf{d}\mathbf{d}^H] = \frac{P_{BS}}{K}\mathbf{I}$, when the sum-power constraint $\mathbb{E}[\|\mathbf{W}_{RF}\mathbf{W}_{BB}\mathbf{d}\|_2] = P_{BS}$ is imposed, we obtain the desired result. \blacksquare

Remark 1. *The above is true when $N_{az}^{(BS)}, N_{az}^{(BS)} \rightarrow \infty$. In the case of finite number of antenna elements, we consider a scheduler where the BS co-schedules K users from clusters such that the above approximation is accurate.*

C. Interference at the Radar due to a Single BS

The radar is assumed to be searching/tracking a target above the horizon ($\phi < 0$) using a receive beamformer $\mathbf{w}_{\text{rad}} \in \mathbb{C}^{M_{\text{rad}} \times 1}$. The interference signal prior to beamforming is $\mathbf{y}_{\text{rad}} = \mathbf{H}_{\text{R}}^H \mathbf{W}_{\text{RF}} \mathbf{W}_{\text{BB}} \mathbf{d}$, where \mathbf{H}_{R} is the high- K_R Rician channel between the BS and the radar from (1). Upon receive beamforming, the interference signal is given by $i_{\text{rad}} = \mathbf{w}_{\text{rad}}^H \mathbf{H}_{\text{R}}^H \mathbf{W}_{\text{RF}} \mathbf{W}_{\text{BB}} \mathbf{d}$. Using equation (1) and simplifying, we get

$$i_{\text{rad}} = \sqrt{\frac{\beta(d)}{K_R+1}} \left(\sqrt{K_R G_{\text{rad}}(\theta_{r,L}, \phi_{r,L})} e^{-j\alpha_0} \mathbf{a}^H(\theta_{t,L}, \phi_{t,L}) + \sum_{i=1}^{N_c} \sqrt{\frac{G_{\text{rad}}(\theta_{r,i}, \phi_{r,i})}{N_c}} \gamma'_i \mathbf{a}^H(\theta_{t,i}, \phi_{t,i}) \right) \times \mathbf{W}_{\text{RF}} \mathbf{W}_{\text{BB}} \mathbf{d}, \quad (3)$$

where $\gamma'_i = \gamma_i^* e^{-j\alpha_i}$, the radar beamforming gain $G_{\text{rad}}(\theta_j, \phi_j) = |\mathbf{w}_{\text{rad}}^H \mathbf{a}(\theta_j, \phi_j)|^2$, and α_0 is the residual phase. The specular component can be ignored if $G_{\text{rad}}(\theta_{r,L}, \phi_{r,L}) \gg G_{\text{rad}}(\theta_{r,i}, \phi_{r,i})$. For a tractable worst-case analytical model, we make the following assumptions.

Assumption 1. (*LoS beamforming gain dominance*) *The radar is scanning above the horizon with $\mathbf{w}_{\text{rad}} = \frac{\mathbf{a}(\theta_{\text{rad}}, \phi_{\text{rad}})}{\sqrt{M_{\text{rad}}}}$ such that $G_{\text{rad}}(\theta_{r,L}, \phi_{r,L}) \gg G_{\text{rad}}(\theta_{r,i}, \phi_{r,i}) \forall 1 \leq i \leq N_c$.*

Assumption 2. (*Boresight assumption*) *Boresight of the antenna array of each massive MIMO BS is aligned along the direction of radar ($\theta_{t,L} = 0$) as shown in Fig. 1b².*

Assumption 3. *The cellular downlink is exactly co-channel with the radar system, and radar and cellular operating bandwidths are equal. Hence, the frequency-dependent rejection (FDR) factor of the radar is unity³.*

²As we will discuss in Appendix A, Assumption 2 facilitates the worst-case analysis of average interference.

³The FDR is dependent on the radar receiver architecture, spectrum of the interfering signal, and is independent of other parameters. The interference power at the radar is inversely proportional to the FDR. Interested readers are referred to [26] for more details.

Assumption 4. In each cell, the scheduler allocates resources to users in different clusters, where all but one cluster has disjoint angular support with the boresight of the BS URA.

Based on the above assumptions, we have the following lemma.

Lemma 1. The interference to the radar from each BS is only due to data transmissions towards a single cluster whose angular support overlaps with the boresight of the URA.

Proof. Let the K clusters have azimuth and elevation angles of support given by Θ_k and Φ_k respectively, for $1 \leq k \leq K$. In the asymptotic regime, if there is only one k such that $\Theta_k \cap \{0^\circ\} \neq \emptyset$, then we get $\mathbf{a}^H(\theta_{t,L}, \phi_{t,L}) \mathbf{w}_{\text{RF},j} \approx 0$ for $j \neq k$ and $\mathbf{a}^H(\theta_{t,L}, \phi_{t,L}) \mathbf{w}_{\text{RF},k} \neq 0$ [4]. The cluster that has its angular support overlapping with the BS boresight is termed as the ‘‘Dominant Interfering User Cluster’’ (DIUC). ■

Based the above, we have the following key result.

Theorem 1. The worst-case average interference power at the radar due to the DIUC is

$$\bar{I}_{\text{rad}} < I_{\text{rad}}^{(\text{w})} = \frac{\beta(d) G_{\text{rad}}(\theta_{\text{rad}}, \phi_{\text{rad}}, \theta_{r,L}, \phi_{r,L}) |\mathbf{a}^H(0, \phi_{t,L}) \mathbf{a}(\theta_k, \phi_k)|^2 P_{BS}}{M_{BS} K}, \quad (4)$$

where $G_{\text{rad}}(\theta_{\text{rad}}, \phi_{\text{rad}}, \theta_{r,L}, \phi_{r,L}) = \frac{|\mathbf{a}^H(\theta_{\text{rad}}, \phi_{\text{rad}}) \mathbf{a}(\theta_{r,L}, \phi_{r,L})|^2}{M_{\text{rad}}}$.

Proof. Under the realistic assumption that each MPC is uncorrelated with the others, the average interference power $\bar{I}_{\text{rad}} = \mathbb{E}[|i_{\text{rad}}|^2]$ is given by

$$\bar{I}_{\text{rad}} = \frac{\beta(d)}{K_R + 1} \left(K_R G_{\text{rad}}(\theta_{\text{rad}}, \phi_{\text{rad}}, \theta_{r,L}, \phi_{r,L}) \mathbb{E}[\|\mathbf{a}^H(0, \phi_{t,L}) \mathbf{W}_{\text{RF}} \mathbf{W}_{\text{BB}} \mathbf{d}\|_2^2] + \sum_{i=1}^{N_c} \frac{G_{\text{rad}}(\theta_{\text{rad}}, \phi_{\text{rad}}, \theta_{r,i}, \phi_{r,i}) \mathbb{E}[\gamma_i'^2 \|\mathbf{a}^H(\theta_{t,i}, \phi_{t,i}) \mathbf{W}_{\text{RF}} \mathbf{W}_{\text{BB}} \mathbf{d}\|_2^2]}{N_c} \right). \quad (5)$$

Using Assumption 1, we get $\bar{I}_{\text{rad}} < \beta(d) G_{\text{rad}}(\theta_{\text{rad}}, \phi_{\text{rad}}, \theta_{r,L}, \phi_{r,L}) \cdot \mathbb{E}[\|\mathbf{a}^H(\theta_{t,L}, \phi_{t,L}) \mathbf{W}_{\text{RF}} \mathbf{W}_{\text{BB}} \mathbf{d}\|_2^2]$ since $\mathbb{E}[|\gamma_i'|^2] = 1$. In addition, by Proposition 1, Assumption 2 and Lemma 1, we get $\bar{I}_{\text{rad}} < \mathbb{E}[\|\mathbf{a}^H(0, \phi_{t,L}) \mathbf{w}_{\text{RF},k} d_k\|^2] \beta(d) G_{\text{rad}}(\theta_{\text{rad}}, \phi_{\text{rad}}, \theta_{r,L}, \phi_{r,L})$. Finally, using $\mathbb{E}[|d_k|^2] = P_{BS}/K$ and substituting the RF beamformer for the DIUC, we obtain the desired result. ■

In summary, the worst-case average interference in high- K_R Rician channels in the asymptotic regime resembles the Friis transmission equation, with the power scaled by the beamforming gains, and the power allocation factor to the DIUC. With this general result, we analyze the average interference due to the cellular network in the next section.

III. AVERAGE INTERFERENCE POWER AT THE RADAR DUE TO THE MASSIVE-MIMO CELLULAR DOWNLINK

We consider a single radar located at the origin, and model the spatial distribution of the massive MIMO BSs as a homogeneous PPP Φ_{BS} , of intensity λ_{BS} . The set of locations in the exclusion zone of radius r_{exc} is denoted by the set $\mathcal{A}_{\text{exc}} = \{(x, y) | (x^2 + y^2) \leq r_{\text{exc}}^2\} \subset \mathbb{R}^2$, in which the BSs are prohibited from operating. The BS locations in the interference region is denoted by the set $\Phi_{\text{int}} = \Phi_{\text{BS}} \setminus \mathcal{A}_{\text{exc}}$. While the range of azimuth of a randomly selected point in the cell is independent of the cell size, the elevation angle depends on the cell size and hence, on λ_{BS} . Compared to prior works [26], [27], which focus on beamforming in the azimuth, mathematical modeling of elevation beamforming presents technical challenges due to (a) lack of radial symmetry in the PV cell, (b) possibility of arbitrarily large PV cells, and (c) correlation between the shapes and sizes of adjacent cells, which can affect the *joint elevation distribution*. It is worthwhile to note that even though the presence of correlation hinders the analytical characterization of the *worst-case interference distribution*, it does not impact the *average worst-case interference*. However, the lack of radial symmetry and possibility of arbitrarily large cells need a more thoughtful treatment as far as average interference is concerned. To complicate matters further, the presence of sidelobes in the beamforming pattern makes it non-trivial to represent the worst-case beamforming gain as a function of the cell-size. Below, we develop the techniques to address these technical challenges, and present the worst-case and nominal average interference analysis.

Lemma 2. *For a $N_{\text{az}} \times N_{\text{el}}$ URA with $\lambda/2$ -spacing, if $\phi \in [-\pi/2, \pi/2)$, $0 \leq \phi_{\text{m}} \leq \frac{\pi}{2}$, and $\theta \in [-\pi/2, \pi/2)$, then the upper bound of the beamforming gain is given by*

$$G_{\text{BS}}^{(\max)}(\phi, \phi_{\text{m}}) = \max_{\substack{\phi_k \in [\phi_{\text{m}}, \pi/2) \\ \theta_k \in [-\pi/2, \pi/2)}} G_{\text{BS}}(\theta, \phi, \theta_k, \phi_k) = \begin{cases} N_{\text{az}}N_{\text{el}}, & \text{if } \phi_{\text{m}} \leq \phi, \\ G_{\text{BS}}(0, \phi, 0, \phi_{\text{m}}), & \text{if } \sin \phi_{\text{m}} \leq \frac{1+N_{\text{el}} \sin \phi}{N_{\text{el}}} \\ \frac{N_{\text{az}}}{N_{\text{el}} \sin^2 \left(\frac{\pi(\sin \phi_{\text{m}} - \sin \phi)}{2} \right)}, & \text{otherwise} \end{cases} \quad (6)$$

where $G_{\text{BS}}(\theta, \phi, \theta_k, \phi_k) = \frac{1}{N_{\text{az}}N_{\text{el}}} |\mathbf{a}^H(\theta, \phi) \mathbf{a}(\theta_k, \phi_k)|^2$.

Proof. See Appendix A. ■

A. Circumcircle-based Cell (CBC) Model

To induce radial symmetry in the setup, the Voronoi cell needs to be modeled as a circle. When beamforming in the azimuthal direction of the radar, the worst-case interference occurs when the BS serving a user beamforms as close to horizon as possible, along which the radar is located. This corresponds to the scenario where the BS beamforms to the *farthest point in the cell*, according to Lemma 2. Since the circumradius determines the distance to the farthest point in a cell, we propose a circumcircle-based construction as shown in Fig. 2, with the following probability density function.

Proposition 2. *The probability density function of the circumradius r_c ($r_c > 0$) of a Poisson-Voronoi cell is*

$$\begin{aligned} f_{R_C}(r_c) &= 8\pi\lambda_{\text{BS}}r_c e^{-4\pi\lambda_{\text{BS}}r_c^2} \left[1 + \sum_{k \geq 1} \left\{ \frac{(-4\pi\lambda_{\text{BS}}r_c^2)^k}{k!} \cdot \left(\frac{\psi_k(r_c)}{8\pi\lambda_{\text{BS}}r_c} - \zeta_k(r_c) \right) - \frac{(-4\pi\lambda_{\text{BS}}r_c^2)^{k-1}\zeta_k(r_c)}{(k-1)!} \right\} \right], \\ \zeta_k(r_c) &= \int_{\|\mathbf{u}\|_1=1, \mathbf{u}_i \in [0,1]} \left[\prod_{i=1}^k F(u_i) \right] e^{4\pi\lambda_{\text{BS}}r_c^2 \sum_{i=1}^k \int_0^{u_i} F(t) dt} d\mathbf{u}, \\ \psi_k(r) &= \frac{d\zeta_k(r)}{dr}, \text{ and } F(t) = \sin^2(\pi t) \mathbb{1}(0 \leq t \leq \frac{1}{2}) + \mathbb{1}(t > \frac{1}{2}), \end{aligned} \quad (7)$$

where $\mathbb{1}(\cdot)$ denotes the indicator function.

Proof. The result is obtained by differentiating the CDF of the circumradius ($F_{R_C}(r_c)$) [36] w.r.t. r_c using Leibniz's rule. ■

Using $f_{R_C}(r_c)$ and Lemma 2, we obtain the upper bound on the average interference in the following key result.

Theorem 2. *The worst-case average interference at the radar is given by*

$$\begin{aligned} \bar{I}_{\text{rad,c}} &= \frac{\lambda_{\text{BS}} P_{\text{BS}} PL(r_0)}{K} \int_{-\frac{\pi}{2}}^{\frac{\pi}{2}} \int_{r_{\text{exc}}}^{\infty} \int_0^{\infty} \frac{r G_{\text{rad}}(\theta_{\text{rad}}, \phi_{\text{rad}}, \theta_{r,L}, -\phi_{t,L}(r)) G_{\text{BS}}^{(\text{max})}(\phi_{t,L}(r), \phi_{\text{m}}(r_c))}{(r^2 + (h_{\text{rad}} - h_{\text{BS}})^2)^{\alpha/2}} f_{R_C}(r_c) dr_c dr d\theta_{r,L}, \\ \phi_{t,L}(r) &= \tan^{-1} \left(\frac{h_{\text{BS}} - h_{\text{rad}}}{r} \right), \phi_{\text{m}}(r_c) = \tan^{-1} \left(\frac{h_{\text{BS}}}{r_c} \right). \end{aligned} \quad (8)$$

Proof. See Appendix B. ■

Corollary 1. *The approximate worst-case average interference at the radar is given by*

$$\bar{I}_{\text{rad,c}}^{(\text{app})} = \frac{\lambda_{\text{BS}} P_{\text{BS}} PL(r_0)}{K(\alpha-2)r_{\text{exc}}^{\alpha-2}} \left[\int_{-\frac{\pi}{2}}^{\frac{\pi}{2}} G_{\text{rad}}(\theta_{\text{rad}}, \phi_{\text{rad}}, \theta_{r,L}, 0) d\theta_{r,L} \right] \cdot \left[\int_0^{\infty} G_{\text{BS}}^{(\text{max})}(0, \phi_{\text{m}}(r)) f_{R_C}(r) dr \right]. \quad (9)$$

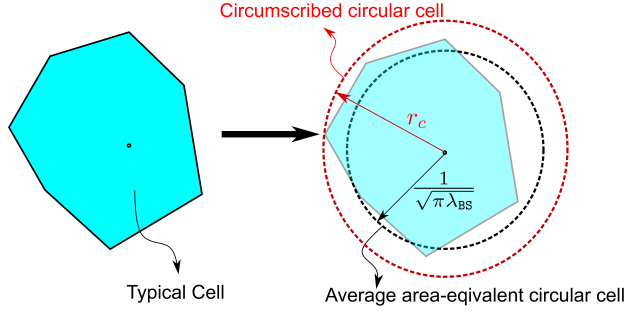


Fig. 2. Radial symmetry can be induced by modeling the Voronoi cell as a (a) circumcircle, or (b) circle of area equal to that of the average typical cell.

Proof. Since $r \gg h_{BS}$ and $r \gg h_{rad}$, we have $\phi_{t,L}(r) = -\phi_{r,L}(r) \approx 0$, and $(r^2 + (h_{BS} - h_{rad})^2)^{\frac{\alpha}{2}} \approx r^\alpha$. Using these approximations in $\bar{I}_{rad,c}$, grouping the integrands, and integrating over r yields the desired result. ■

B. Average Area-Equivalent Circular Cell (AAECC) Model

The circumcircle-based cell model results in a conservative value for average interference. A simpler, more optimistic model is to replace the Voronoi cell by a circle with an area equal to the average area of a typical cell given by $\frac{1}{\lambda_{BS}}$. In this case, the cell radius $r_c = r_a = \frac{1}{\sqrt{\pi\lambda_{BS}}}$, and the nominal average interference is given by the following theorem.

Theorem 3. *The nominal mean and standard deviation of the interference power is*

$$\bar{I}_{rad,a} = \frac{\lambda_{BS} P_{BS} PL(r_0)}{K} \int_{-\frac{\pi}{2}}^{\frac{\pi}{2}} \int_{r_{exc}}^{\infty} \frac{r G_{rad}(\theta_{rad}, \phi_{rad}, \theta_{r,L}, \phi_{r,L}(r)) G_{BS}^{(max)}(\phi_{t,L}(r), \phi_m(r_a))}{(r^2 + (h_{rad} - h_{BS})^2)^{\alpha/2}} dr d\theta_{r,L}, \quad (10)$$

$$\sigma_{rad,a} = \frac{\sqrt{\lambda_{BS}} P_{BS} PL(r_0)}{K} \sqrt{\int_{-\frac{\pi}{2}}^{\frac{\pi}{2}} \int_{r_{exc}}^{\infty} \frac{r^2 G_{rad}^2(\theta_{rad}, \phi_{rad}, \theta_{r,L}, \phi_{r,L}(r)) [G_{BS}^{(max)}(\phi_{t,L}(r), \phi_m(r_a))]^2}{(r^2 + (h_{rad} - h_{BS})^2)^{\alpha}} dr d\theta_{r,L}}. \quad (11)$$

Proof. This model is a special case of Theorem 2, where $f_{R_c}(r_c) = \delta(r_c - \frac{1}{\sqrt{\pi\lambda_{BS}}})$. Using the sifting property of the Dirac delta function $\delta(\cdot)$ in equation (8), we obtain equation (10). The variance is obtained using Campbell's theorem, in a similar manner as Appendix B. ■

Corollary 2. *The approximate nominal average and variance of the interference power is*

$$\bar{I}_{rad,a}^{(app)} = \frac{\lambda_{BS} P_{BS} PL(r_0) G_{BS}^{(max)}(0, \phi_m(r_a))}{K(\alpha - 2) r_{exc}^{\alpha-2}} \int_{-\frac{\pi}{2}}^{\frac{\pi}{2}} G_{rad}(\theta_{rad}, \phi_{rad}, \theta, 0) d\theta,$$

$$\sigma_{rad,a}^{(app)} = \frac{\sqrt{\lambda_{BS}} P_{BS} PL(r_0) G_{BS}^{(max)}(0, \phi_m(r_a))}{\sqrt{(2\alpha - 2) K} r_{exc}^{\alpha-1}} \sqrt{\int_{-\frac{\pi}{2}}^{\frac{\pi}{2}} G_{rad}^2(\theta_{rad}, \phi_{rad}, \theta, 0) d\theta}.$$

Proof. The proof follows the same steps as Corollary 1. ■

C. System Design Insights

1) *Scaling of average interference power with BS density:* From (8) and (10), we see that λ_{BS} impacts the average interference through the linear term and the BS beamforming gain (G_{BS}) term. It is related to the cell size via the circumradius distribution and the average area of the typical cell, which impacts the *minimum elevation angle* (ϕ_{m}). Note that this dependence is not observed in azimuth-only beamforming models. However, when $h_{\text{BS}} \ll r_c$, the elevation angle $\phi_{\text{m}}(r_c) \rightarrow 0$ and hence, $G_{\text{BS}} \rightarrow M_{\text{BS}}$. In this regime, the worst-case average interference power scales linearly with λ_{BS} .

2) *Exclusion Zone Radius:* In practice, exclusion zones are defined based on the average aggregate interference power (for e.g. see [8]). Using Corollaries 1 and 2, for an average interference threshold \bar{I}_{th} and $\alpha > 2$, the worst-case exclusion zone radius ($r_{\text{exc}}^{(\text{w})}$) can be obtained using

$$r_{\text{exc}}^{(\text{w})} \approx \left(\frac{\lambda_{\text{BS}} P_{\text{BS}} P_L(r_0)}{K(\alpha-2)\bar{I}_{\text{th}}} \left[\int_{-\frac{\pi}{2}}^{\frac{\pi}{2}} G_{\text{rad}}(\theta_{\text{rad}}, \phi_{\text{rad}}, \theta, 0) d\theta \right] \cdot \left[\int_0^\infty G_{\text{BS}}^{(\text{max})}(0, \phi_{\text{m}}(r_c)) f_{R_C}(r) dr \right] \right)^{\frac{1}{\alpha-2}}.$$

3) *Constant Gap in Average Interference Predicted by CBC and AAEC Models:* By Corollaries (1) and (2), we observe that the ratio of average interference powers is nearly independent of r_{exc} , given by

$$\eta_{\text{ca}} = \frac{\bar{I}_{\text{rad,c}}^{(\text{app})}}{\bar{I}_{\text{rad,a}}^{(\text{app})}} = \frac{\int_0^\infty G_{\text{BS}}^{(\text{max})}(0, \phi_{\text{m}}(r_c)) f_{R_C}(r_c) dr_c}{G_{\text{BS}}^{(\text{max})}\left(0, \phi_{\text{m}}\left(\frac{1}{\sqrt{\pi\lambda_{\text{BS}}}}\right)\right)}.$$

Note that $\eta_{\text{ca}} \rightarrow 1$ when $h_{\text{BS}}\sqrt{\pi\lambda_{\text{BS}}} \rightarrow 0$ due to BS gain saturation.

In the next section, we analyze the distribution of interference at the radar due to the massive MIMO cellular downlink.

IV. DISTRIBUTION OF MASSIVE-MIMO DOWNLINK INTERFERENCE AT THE RADAR

To study the impact of large-scale network interference on aggregate radar performance metrics such as *spatial probability of detection/false alarm* [28], deriving the distribution of interference due to spatial randomness in the BS locations is a key intermediate step. To accomplish this, a common approach in stochastic geometry literature is to characterize the Laplace transform of the interference distribution, which leverages the presence of an exponential term in Rayleigh fading channels [42]. However in our case, the Laplace transform method is not applicable, since

we ignore the small scale fading term in the high- K_R Rician channel to model the worst-case interference scenario. To obtain useful results, we use the dominant interferer approximation [25], [37], [38], [39] described below.

Assumption 5. *In the cellular network, if the interference power due to the dominant interfering BS is I_{dom} , and that due to the rest of the network is I_{rest} , then the total interference power (I_{tot}) is approximated by the sum of the dominant BS interference power and the average interference power due to the rest of the network, conditioned on the dominant interference power. Mathematically, it can be written as*

$$I_{\text{tot}} \approx I_{\text{dom}} + \mathbb{E}_{I_{\text{dom}}}[I_{\text{rest}}|I_{\text{dom}}], \quad (12)$$

In the case of omnidirectional reception at the receiver, the distribution of I_{dom} is directly related to the distance distribution of the nearest transmitter in the point process [43], since the contour of equal interference power is a circle [39]. However in our case, receive beamforming at the radar distorts radial symmetry, since received power depends on the azimuth and elevation angle, in addition to the distance from the interfering BS. Therefore, the first step is to characterize the contour curves of equal interference power, which is fundamental to calculating the void probability [42] and hence, the distribution of I_{dom} . In the rest of this paper, we assume cell-edge beamforming in the AAEC model to derive useful expressions for the interference distribution. In the following subsection, we characterize the equal interference contours in our radar-cellular coexistence scenario.

A. Equal Interference Contours in Radar-Massive MIMO Spectrum Sharing

The equal interference power contour $\mathcal{C}(I)$ contains points (r, θ) such that the received power due to a transmitter at location $(r, \theta) \in \mathcal{C}(I)$ is I . The following proposition denotes the contour lying outside the exclusion zone in the radar-cellular spectrum sharing scenario.

Proposition 3. *Under the AAEC model, the contour $\mathcal{C}(I_{\text{dom}})$ is given by*

$$\begin{aligned} \mathcal{C}(I_{\text{dom}}) = & \left\{ (r, \theta) \left| G_{\text{rad}}(\theta_{\text{rad}}, \phi_{\text{rad}}, \theta, \phi(r)) G_{\text{BS}}^{(\text{max})}(-\phi(r), \phi_m(1/\sqrt{\pi\lambda_{\text{BS}}})) r^{-\alpha} = \frac{KI_{\text{dom}}}{PL(r_0)P_{\text{BS}}}, \right. \right. \\ & \left. \left. r \geq r_{\text{exc}}, \theta \in \left[-\frac{\pi}{2}, \frac{\pi}{2}\right] \right\} \right. \\ & \text{where } \phi(r) = \tan^{-1}\left(\frac{h_{\text{rad}} - h_{\text{BS}}}{r}\right), \phi_m(r') = \tan^{-1}(h_{\text{BS}}/r'). \end{aligned} \quad (13)$$

Proof. The worst-case interference power due to a massive MIMO BS at (r, θ) is given by (4).

Since the BSs inside the exclusion zone are inactive, the contour can be written as

$$\mathcal{C}(I_{\text{dom}}) = \left\{ (r, \theta) \left| \frac{PL(r_0)P_{BS}G_{\text{rad}}(\theta_{\text{rad}}, \phi_{\text{rad}}, \theta, \phi(r))G_{\text{BS}}^{(\text{max})}(-\phi(r), \phi_{\text{m}}(1/\sqrt{\pi\lambda_{\text{BS}}}))}{Kr^\alpha} = I_{\text{dom}}, \right. \right. \\ \left. \left. r \geq r_{\text{exc}}, \theta \in \left[-\frac{\pi}{2}, \frac{\pi}{2} \right] \right\}. \quad (14)$$

Rearranging the terms independent of (r, θ) , we obtain the desired result. \blacksquare

In the case of large exclusion zone radii, we show in the following lemma that the equal-interference contour can be represented by the *farthest distance between the contour and the radar*, when conditioned on the radar beamforming vector.

Lemma 3. *Under the AAEC model, when $h_{\text{BS}} \ll r_{\text{exc}}$ and $h_{\text{rad}} \ll r_{\text{exc}}$, the equal interference contour is given by*

$$\mathcal{C}(I_{\text{dom}}) = \left\{ (r, \theta) \left| r = r_{\text{dom}} \left[\frac{\sin\left(\frac{\pi}{2}N_{\text{az}}^{(\text{rad})}(\sin\theta_{\text{rad}}\phi_{\text{rad}} - \sin\theta)\right)}{N_{\text{az}}^{(\text{rad})}\sin\left(\frac{\pi}{2}(\sin\theta_{\text{rad}}\phi_{\text{rad}} - \sin\theta)\right)} \right]^{2/\alpha}, r_{\text{dom}} \geq r_{\text{exc}}, \theta \in \left[-\frac{\pi}{2}, \frac{\pi}{2} \right] \right\}, \\ \text{where } I_{\text{dom}} \triangleq \frac{P_{BS}PL(r_0)G_{\text{BS}}^{(\text{max})}(0, \phi_{\text{m}}(1/\sqrt{\pi\lambda_{\text{BS}}}))}{Kr_{\text{dom}}^\alpha} \cdot \frac{N_{\text{az}}^{(\text{rad})}\sin^2\left(\frac{\pi}{2}N_{\text{el}}^{(\text{rad})}\sin\phi_{\text{rad}}\right)}{N_{\text{el}}^{(\text{rad})}\sin^2\left(\frac{\pi}{2}\sin\phi_{\text{rad}}\right)}. \quad (15)$$

Proof. Please refer to Appendix C. \blacksquare

From equation (15), we observe that there is a bijection between r_{dom} , the farthest distance of the contour from the radar, and interference power I_{dom} under the AAEC model when $h_{\text{BS}} \ll r_{\text{exc}}$ and $h_{\text{rad}} \ll r_{\text{exc}}$, which are both reasonable assumptions in practice. Therefore, we can equivalently denote the *equal interference contour* by $\mathcal{C}(r_{\text{dom}})$, when conditioned on the radar beamforming vector. Fig. 3a shows an example of the equal interference contour, which resembles a horizontal cross section of the radar's 3D beamforming pattern at elevation $\phi = 0^\circ$. In the following subsection, we derive the distribution of the dominant interference power I_{dom} .

B. Distribution of I_{dom}

The distribution of I_{dom} is related to the void probability of a PPP in the region outside the exclusion zone enclosed by the equal interference contour [42], as shown in Fig. 3b. In the following key result, we derive an analytical expression for the area of this region $A(r_{\text{dom}})$.

Lemma 4. *Under the AAEC model, when $r_{\text{exc}} \gg h_{\text{BS}}$ and $r_{\text{exc}} \gg h_{\text{rad}}$, $A(r_{\text{dom}})$ is given by*

$$A(r_{\text{dom}}) = \frac{1}{2} \int_{-\frac{\pi}{2}}^{\frac{\pi}{2}} \max\left(r_{\text{exc}}^2, r_{\text{dom}}^2 \left[\frac{\sin\left(\frac{\pi}{2}N_{\text{az}}^{(\text{rad})}(\sin\theta_{\text{rad}}\cos\phi_{\text{rad}} - \sin\theta)\right)}{N_{\text{az}}^{(\text{rad})}\sin\left(\frac{\pi}{2}(\sin\theta_{\text{rad}}\cos\phi_{\text{rad}} - \sin\theta)\right)} \right]^{\frac{4}{\alpha}}\right) d\theta - \frac{\pi r_{\text{exc}}^2}{2}, \quad (16)$$

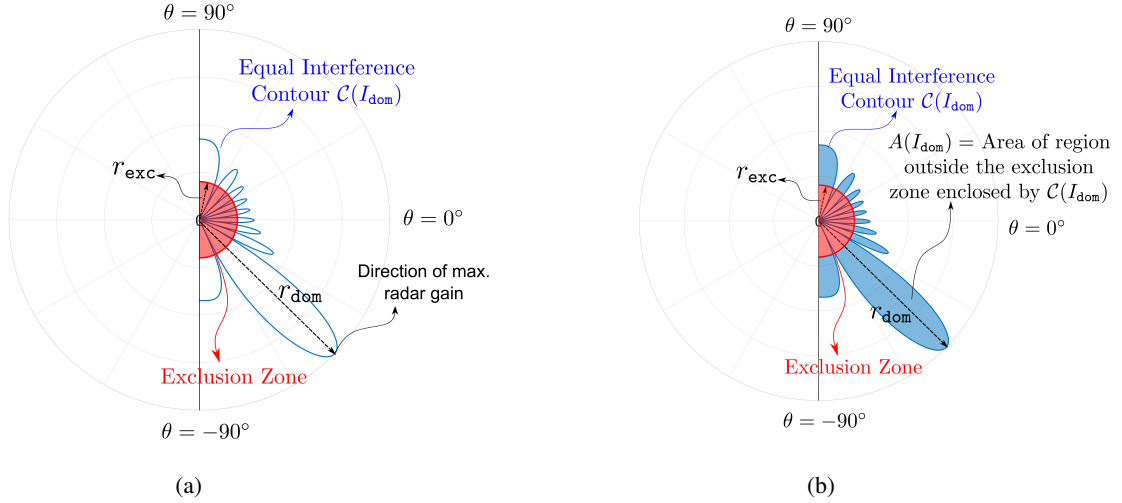


Fig. 3. (a) Schematic of the equal interference power contour $\mathcal{C}(I_{\text{dom}})$ in polar coordinates, for a radar with $N_{\text{az}}^{(\text{rad})} = N_{\text{az}}^{(\text{rad})} = 8$, scanning a target at $(\theta_{\text{rad}}, \phi_{\text{rad}}) = (-60^\circ, -5^\circ)$, with $\alpha = 3.5$, $r_{\text{exc}} = 4$ km, and $r_1 = 20$ km. Distance of the farthest point on the contour is denoted by r_{dom} . (b) Area of the region outside the exclusion zone but enclosed by $\mathcal{C}(I_{\text{dom}})$ is denoted by $A(I_{\text{dom}})$.

Proof. Please refer Appendix D. ■

Using the above result, the density and distribution of r_{dom} is characterized in the following lemma.

Lemma 5. *The distribution and density function of r_{dom} are given by*

$$F_{R_{\text{dom}}}(r_{\text{dom}}) = 1 - \exp\left(-\frac{\lambda_{\text{BS}}}{2} \int_{-\frac{\pi}{2}}^{\frac{\pi}{2}} \max(r_{\text{exc}}^2, \tilde{r}_{\text{dom}}^2(\theta)) d\theta + \frac{\pi \lambda_{\text{BS}} r_{\text{exc}}^2}{2}\right), \quad (17)$$

$$f_{R_{\text{dom}}}(r_{\text{dom}}) = \lambda_{\text{BS}} \left[\int_{-\frac{\pi}{2}}^{\frac{\pi}{2}} r_{\text{dom}} \left[\frac{\sin\left(\frac{\pi}{2} N_{\text{az}}^{(\text{rad})} (\sin \theta_{\text{rad}} \cos \phi_{\text{rad}} - \sin \theta)\right)}{N_{\text{az}}^{(\text{rad})} \sin\left(\frac{\pi}{2} (\sin \theta_{\text{rad}} \cos \phi_{\text{rad}} - \sin \theta)\right)} \right]^{\frac{4}{\alpha}} \cdot \mathbb{1}[\tilde{r}_{\text{dom}}(\theta) \geq r_{\text{exc}}] d\theta \right] \cdot \exp\left(-\frac{\lambda_{\text{BS}}}{2} \int_{-\frac{\pi}{2}}^{\frac{\pi}{2}} \max(r_{\text{exc}}^2, \tilde{r}_{\text{dom}}^2(\theta)) d\theta + \frac{\pi \lambda_{\text{BS}} r_{\text{exc}}^2}{2}\right), \quad (18)$$

where $\tilde{r}_{\text{dom}}(\theta) \triangleq r_{\text{dom}} \left[\frac{\sin\left(\frac{\pi}{2} N_{\text{az}}^{(\text{rad})} (\sin \theta_{\text{rad}} \cos \phi_{\text{rad}} - \sin \theta)\right)}{N_{\text{az}}^{(\text{rad})} \sin\left(\frac{\pi}{2} (\sin \theta_{\text{rad}} \cos \phi_{\text{rad}} - \sin \theta)\right)} \right]^{\frac{2}{\alpha}}$, and $\mathbb{1}[\cdot]$ is the indicator function.

Proof. Please refer Appendix E. ■

Since a bijection exists between r_{dom} and I_{dom} , the density and distribution of I_{dom} can be derived similar to Lemma 5, and is given in the following result.

Lemma 6. *The distribution and density of I_{dom} under the AAEC model are given by*

$$F_{I_{\text{dom}}}(i_{\text{dom}}) = \exp\left(-\frac{\lambda_{\text{BS}}\kappa^{\frac{2}{\alpha}}}{2}\left[\int_{-\frac{\pi}{2}}^{\frac{\pi}{2}} \max(I_{\text{exc}}^{-2/\alpha}, \tilde{i}_{\text{dom}}^{-2/\alpha}(\theta))d\theta - \pi I_{\text{exc}}^{-2/\alpha}\right]\right), \quad (19)$$

$$f_{I_{\text{dom}}}(i_{\text{dom}}) = \frac{\lambda_{\text{BS}}\kappa^{2/\alpha}}{\alpha}\left[\int_{-\frac{\pi}{2}}^{\frac{\pi}{2}} i_{\text{dom}}^{-(\alpha+2)/\alpha}\left[\frac{\sin\left(\frac{\pi}{2}N_{\text{az}}^{(\text{rad})}(\sin\theta_{\text{rad}}\cos\phi_{\text{rad}}-\sin\theta)\right)}{N_{\text{az}}^{(\text{rad})}\sin\left(\frac{\pi}{2}(\sin\theta_{\text{rad}}\cos\phi_{\text{rad}}-\sin\theta)\right)}\right]^{\frac{2}{\alpha}}\mathbb{1}[\tilde{i}_{\text{dom}}(\theta)\leq I_{\text{exc}}]d\theta\right] \exp\left(-\frac{\lambda_{\text{BS}}\kappa^{\frac{2}{\alpha}}}{2}\left[\int_{-\frac{\pi}{2}}^{\frac{\pi}{2}} \max(I_{\text{exc}}^{-2/\alpha}, \tilde{i}_{\text{dom}}^{-2/\alpha}(\theta))d\theta - \pi I_{\text{exc}}^{-2/\alpha}\right]\right), \quad (20)$$

where $\kappa = \frac{P_{\text{BS}}PL(r_0)G_{\text{BS}}^{(\text{max})}(0, \phi_{\text{m}}(1/\sqrt{\pi\lambda_{\text{BS}}}))}{K} \cdot \frac{N_{\text{az}}^{(\text{rad})}\sin^2\left(\frac{\pi}{2}N_{\text{e1}}^{(\text{rad})}\sin\phi_{\text{rad}}\right)}{N_{\text{e1}}^{(\text{rad})}\sin^2\left(\frac{\pi}{2}\sin\phi_{\text{rad}}\right)}$, and $\tilde{i}_{\text{dom}}(\theta) = \frac{i_{\text{dom}}\frac{N_{\text{az}}^{(\text{rad})}\sin\left(\frac{\pi}{2}(\sin\theta_{\text{rad}}\cos\phi_{\text{rad}}-\sin\theta)\right)}{\sin\left(\frac{\pi}{2}N_{\text{az}}^{(\text{rad})}(\sin\theta_{\text{rad}}\cos\phi_{\text{rad}}-\sin\theta)\right)}}{i_{\text{dom}}\frac{N_{\text{az}}^{(\text{rad})}\sin\left(\frac{\pi}{2}(\sin\theta_{\text{rad}}\cos\phi_{\text{rad}}-\sin\theta)\right)}{\sin\left(\frac{\pi}{2}N_{\text{az}}^{(\text{rad})}(\sin\theta_{\text{rad}}\cos\phi_{\text{rad}}-\sin\theta)\right)}}$.

Proof. From equation (15), we observe that the bijection between the dominant interference power I_{dom} and the corresponding farthest contour distance r_{dom} can be represented by $I_{\text{dom}} = \kappa r_{\text{dom}}^{-\alpha}$. Since I monotonically decreases with increasing r , the CDF of I_{dom} is given by $\mathbb{P}[I_{\text{dom}} \leq i_{\text{dom}}] = \mathbb{P}[R_{\text{dom}} \geq r_{\text{dom}}]$. Using equation (17), we get $F_{I_{\text{dom}}}(i_{\text{dom}}) = \exp(-\lambda_{\text{BS}}A(r_{\text{dom}}))$ for $r_{\text{dom}} \geq r_{\text{exc}}$. Using the bijection and simplifying, we get the desired CDF. The density is obtained in a similar manner as Lemma 5, by differentiating equation (19) w.r.t. i_{dom} . ■

C. Total Interference Power at the Radar

Since r_{dom} can equivalently represent the equal interference contour $\mathcal{C}(I_{\text{dom}})$, we use Lemma 5 in the following result to approximately characterize the total interference power at the radar, using the dominant interferer method.

Theorem 4. *The total interference power at the radar under the AAEC model and Assumption 5 is given by*

$$I_{\text{tot}}(r_{\text{dom}}) = \kappa\left[r_{\text{dom}}^{-\alpha} + \frac{\lambda_{\text{BS}}}{\alpha-2}\int_{-\frac{\pi}{2}}^{\frac{\pi}{2}}\left[\frac{\sin\left(\frac{\pi}{2}N_{\text{az}}^{(\text{rad})}(\sin\theta_{\text{rad}}\cos\phi_{\text{rad}}-\sin\theta)\right)}{N_{\text{az}}^{(\text{rad})}\sin\left(\frac{\pi}{2}(\sin\theta_{\text{rad}}\cos\phi_{\text{rad}}-\sin\theta)\right)}\right]^2\left(\max(r_{\text{exc}}, \tilde{r}_{\text{dom}}(\theta))\right)^{-\alpha+2}d\theta\right]. \quad (21)$$

Proof. Please refer Appendix F. ■

Remark 2. *It is worthwhile to note that $I_{\text{tot}}(r_{\text{dom}})$ has finite support, i.e. $I_{\text{tot}} \in (0, I_{\text{exc}} + \bar{I}_{\text{rad,a}})$. This is because the maximum dominant interference power is upper bounded by I_{exc} , and the corresponding conditional average interference power is $\bar{I}_{\text{rad,a}}$ (equation 10).*

In the following corollary, we prove that a bijection exists between $I_{\text{tot,DI}}$ and r_{dom} .

Corollary 3. *Under the dominant interferer approximation, I_{tot} monotonically decreases with r_{dom} .*

Proof. The proof follows by showing that both terms in equation (21) monotonically decrease with r_{dom} . It is clear that I_{dom} monotonically decreases with increasing r_{dom} . In addition, we note that $\mathcal{A}(r_{\text{dom}}) \subset \mathcal{A}(kr_{\text{dom}}) \forall k \in \mathbb{R}, k > 1$. As a result, the integration region and hence, the average interference power in equation (36) shrinks as r_{dom} increases. Therefore, the sum of these terms decreases monotonically with r_{dom} . ■

Hence, a bijection exists between r_{dom} and I_{tot} under the dominant interferer approximation. Unfortunately, the mapping from I_{tot} to r_{dom} cannot be expressed in closed-form. Hence for tractability, we use the distribution of r_{dom} in place of I_{tot} to characterize the radar performance metrics in the following section.

V. CHARACTERIZATION OF RADAR PERFORMANCE METRICS

In this section, we use the distribution of r_{dom} to characterize the impact of cellular interference on the radar's detection and false alarm performance in a target tracking scenario.

A. Radar Received Signal Model

In the presence of cellular interference and noise, the aggregate received signal depends on the presence or absence of a target at $(\theta_{\text{rad}}, \phi_{\text{rad}})$, when the radar performs receive beamforming using the weights $\mathbf{w}_{\text{rad}} = \frac{1}{\sqrt{M_{\text{rad}}}} \mathbf{a}(\theta_{\text{rad}}, \phi_{\text{rad}})$. Denoting the received signal post-beamforming at time index n is $y_{\text{rad}}[n]$, we assume that the radar calculates the test statistic $P_{\text{rad}} = \frac{1}{N} \sum_{n=1}^N |y_{\text{rad}}[n]|^2$ in an estimation window of N samples. Let \mathcal{H}_0 denote the hypothesis that there is no target, and \mathcal{H}_1 denote the hypothesis that there is a target. We assume that each BS transmits i.i.d. complex Gaussian signals, and noise is i.i.d. circularly symmetric complex Gaussian. In near-LoS channel conditions, when BSs transmit i.i.d. Gaussian signals, the aggregate interference signal is Gaussian distributed *when conditioned on the BS locations* Φ_{int} . Thus, the received signal under each hypothesis can be written as

$$\mathcal{H}_0 : y_{\text{rad},0}[n] = \sqrt{(I_{\text{tot}}(\Phi_{\text{int}}) + \sigma_n^2)} w[n], \quad (22)$$

$$\mathcal{H}_1 : y_{\text{rad},1}[n] = \sqrt{(I_{\text{tot}}(\Phi_{\text{int}}) + \sigma_n^2)} w[n] + \sqrt{P_{\text{tar}}} e^{j\alpha[n]}, \quad (23)$$

where $I_{\text{tot}}(\Phi_{\text{int}})$ is the aggregate interference power, σ_n^2 denotes the noise variance, $w[n] \sim \mathcal{CN}(0, 1)$, P_{tar} is the received power due to target scatter, and $\alpha[n]$ is the phase of the target return at time n . Using this system model, we have the following results regarding the distribution of P_{rad} under the two hypotheses.

Lemma 7. *The conditional distributions of the test statistic under the two hypotheses can be expressed as*

$$\begin{aligned}\mathcal{H}_0 : F_{P_{\text{rad},0}}(p|I_{\text{tot}}(\Phi_{\text{int}})) &= \frac{1}{(N-1)!} \gamma_l\left(N, \frac{Np}{I_{\text{tot}}(\Phi_{\text{int}}) + \sigma_n^2}\right), \\ \mathcal{H}_1 : F_{P_{\text{rad},1}}(p|I_{\text{tot}}(\Phi_{\text{int}})) &= 1 - Q_N\left(\sqrt{\frac{2NP_{\text{tar}}}{I_{\text{tot}}(\Phi_{\text{int}}) + \sigma_n^2}}, \sqrt{\frac{2Np}{I_{\text{tot}}(\Phi_{\text{int}}) + \sigma_n^2}}\right),\end{aligned}\quad (24)$$

where $\gamma_l(a, x) = \int_0^x z^{a-1} e^{-z} dz$ is the lower incomplete gamma function, $Q_N(a, b) = \int_b^\infty z^N / a^{N-1} \exp(-(z^2 + a^2)/2) I_{N-1}(az) dz$ is the Marcum Q -function, and $I_{N-1}(z)$ is the modified Bessel function of order $(N-1)$.

Proof. We observe from equation (22) that under hypothesis \mathcal{H}_0 , each sample in the estimation window is i.i.d. complex Gaussian distributed such that $\Re\left(\frac{y_{\text{rad},0}[n]\sqrt{2N}}{\sqrt{I_{\text{tot}}(\Phi_{\text{int}}) + \sigma_n^2}}\right) \sim \mathcal{N}(0, 1)$ and $\Im\left(\frac{y_{\text{rad},0}[n]\sqrt{2N}}{\sqrt{I_{\text{tot}}(\Phi_{\text{int}}) + \sigma_n^2}}\right) \sim \mathcal{N}(0, 1)$ for $n = 1, 2, \dots, N$, where $\Re(\cdot)$ and $\Im(\cdot)$ denote the real and imaginary parts. Taking the squared sum of these terms, we observe that $\frac{2NP_{\text{rad},0}}{I_{\text{tot}}(\Phi_{\text{int}}) + \sigma_n^2}$ is chi-squared distributed with $2N$ degrees of freedom, and the CDF follows accordingly.

Similarly, the received signal samples under \mathcal{H}_1 are independent such that $\Re\left(\frac{y_{\text{rad},1}[n]\sqrt{2N}}{\sqrt{I_{\text{tot}}(\Phi_{\text{int}}) + \sigma_n^2}}\right) \sim \mathcal{N}\left(\frac{\sqrt{2NP_{\text{tar}}}\cos(\alpha[n])}{\sqrt{I_{\text{tot}}(\Phi_{\text{int}}) + \sigma_n^2}}, 1\right)$ and $\Im\left(\frac{y_{\text{rad},1}[n]\sqrt{2N}}{\sqrt{I_{\text{tot}}(\Phi_{\text{int}}) + \sigma_n^2}}\right) \sim \mathcal{N}\left(\frac{\sqrt{2NP_{\text{tar}}}\sin(\alpha[n])}{\sqrt{I_{\text{tot}}(\Phi_{\text{int}}) + \sigma_n^2}}, 1\right)$, for $n = 1, 2, \dots, N$. Taking the squared sum of these terms, we see that $\frac{2NP_{\text{rad},1}}{I_{\text{tot}}(\Phi_{\text{int}}) + \sigma_n^2}$ has a non-central chi-squared distribution with $2N$ degrees of freedom and non-central parameter $\lambda = \frac{2NP_{\text{tar}}}{I_{\text{tot}}(\Phi_{\text{int}}) + \sigma_n^2}$. The CDF follows accordingly. \blacksquare

Corollary 4. *When $N \rightarrow \infty$, the conditional distributions of the test statistic under the two hypotheses become*

$$\begin{aligned}\mathcal{H}_0 : F_{P_{\text{rad},0}}(p|I_{\text{tot}}(\Phi_{\text{int}})) &= 1 - Q\left(\frac{\sqrt{N}(p - I_{\text{tot}}(\Phi_{\text{int}}) - \sigma_n^2)}{I_{\text{tot}}(\Phi_{\text{int}}) + \sigma_n^2}\right), \\ \mathcal{H}_1 : F_{P_{\text{rad},1}}(p|I_{\text{tot}}(\Phi_{\text{int}})) &= 1 - Q\left(\frac{\sqrt{N}(p - P_{\text{tar}} - I_{\text{tot}}(\Phi_{\text{int}}) - \sigma_n^2)}{\sqrt{(P_{\text{tar}} + I_{\text{tot}}(\Phi_{\text{int}}) + \sigma_n^2)^2 - P_{\text{tar}}^2}}\right),\end{aligned}\quad (25)$$

where $Q(x) = 1/\sqrt{2\pi} \int_x^\infty \exp(-u^2/2) du$ is the Q -function.

Proof. Observe that when $y_i \stackrel{\text{i.i.d.}}{\sim} \mathcal{CN}(0, \sigma^2)$, $i = 1, 2, \dots, N$ and $N \rightarrow \infty$, we have $\frac{1}{N} \sum_{i=1}^N |y_i|^2 \sim \mathcal{N}(\sigma^2, N^{-1}\sigma^4)$ [40]. Hence, the CDF of $P_{\text{rad},0}$ follows by replacing σ^2 by $\text{Var}(y_{\text{rad},0}[n]) = I_{\text{tot}}(\Phi_{\text{int}}) + \sigma_n^2$.

On the other hand, the mean and variance of $|y_{\text{rad},1}[n]|^2$ is finite and is given by $\mathbb{E}[|y_{\text{rad},1}[n]|^2] = P_{\text{tar}} + I_{\text{tot}} + \sigma_n^2$ and $\text{Var}(|y_{\text{rad},1}[n]|^2) = (I_{\text{tot}} + \sigma_n^2)^2 + 2P_{\text{tar}}(I_{\text{tot}} + \sigma_n^2)$ respectively, for $n = 1, 2, \dots, N$. Using the central limit theorem, the distribution of $P_{\text{rad},1}$ approaches a Gaussian distribution with mean $\mathbb{E}[P_{\text{rad},1}] = P_{\text{tar}} + I_{\text{tot}} + \sigma_n^2$ and variance $\text{Var}(P_{\text{rad},1}) = N^{-1}[(I_{\text{tot}} + \sigma_n^2)^2 + 2P_{\text{tar}}(I_{\text{tot}} + \sigma_n^2)]$, when $N \rightarrow \infty$. The CDF follows accordingly. ■

B. Radar Performance Metrics

When conditioned on the interference $I_{\text{tot}}(\Phi_{\text{int}})$, noise power σ_n^2 , and the detection threshold P_{th} , the probability of detection (P_d) and false alarm (P_{fa}) are calculated using

$$P_d = \mathbb{P}[P_{\text{rad}} > P_{\text{th}} | \mathcal{H}_1, I_{\text{tot}}(\Phi_{\text{int}}), \sigma_n^2], \quad P_{\text{fa}} = \mathbb{P}[P_{\text{rad}} > P_{\text{th}} | \mathcal{H}_0, I_{\text{tot}}(\Phi_{\text{int}}), \sigma_n^2]. \quad (26)$$

We assume that the noise variance is constant. However, since the cellular downlink network is a PPP, we are interested in a spatially averaged variant of these probabilities. These are termed as the spatial detection probability (\bar{P}_d), and the probability of spatial false alarm (\bar{P}_{fa}), which are defined as [28]

$$\begin{aligned} \bar{P}_d &= \int_0^\infty \mathbb{P}[P_{\text{rad}} > P_{\text{th}} | \mathcal{H}_1, I_{\text{tot}}] f_{I_{\text{tot}}}(x) dx, \\ \bar{P}_{\text{fa}} &= \int_0^\infty \mathbb{P}[P_{\text{rad}} > P_{\text{th}} | \mathcal{H}_0, I_{\text{tot}}] f_{I_{\text{tot}}}(x) dx. \end{aligned} \quad (27)$$

where P_{rad} is the test statistic, and $f_{I_{\text{tot}}}(\cdot)$ is the density functions of the cellular interference power. For notational simplicity, the dependence of I_{tot} on the random BS locations (Φ_{int}) is omitted. In the following key result, we provided a tractable approximation to the spatial detection and false alarm probabilities.

Theorem 5. *The probability of spatial detection and spatial false alarm under Assumption 5 is given by*

$$\begin{aligned} \bar{P}_{\text{fa}, \chi^2} &= 1 - \frac{1}{(N-1)!} \int_{r_{\text{exc}}}^\infty \gamma_l \left(N, \frac{NP_{\text{th}}}{I_{\text{tot}, \text{DI}}(r_{\text{dom}}) + \sigma_w^2} \right) f_{R_{\text{dom}}}(r_{\text{dom}}) dr_{\text{dom}}, \\ \bar{P}_{d, \chi^2} &= \int_{r_{\text{exc}}}^\infty Q_N \left(\sqrt{\frac{2NP_{\text{tar}}}{I_{\text{tot}, \text{DI}}(r_{\text{dom}}) + \sigma_w^2}}, \sqrt{\frac{2NP_{\text{th}}}{I_{\text{tot}, \text{DI}}(r_{\text{dom}}) + \sigma_w^2}} \right) f_{R_{\text{dom}}}(r_{\text{dom}}) dr_{\text{dom}}, \end{aligned} \quad (28)$$

where $f_{R_{\text{dom}}}(\cdot)$ is the PDF of r_{dom} (equation (18)), and $I_{\text{tot,DI}}$ is the total interference power under the dominant interferer approximation (equation (21)).

Proof. Please refer Appendix G. ■

Corollary 5. When $N \rightarrow \infty$, the probability of spatial detection and spatial false alarm under Assumption 5 can be written as

$$\begin{aligned}\bar{P}_{\text{fa,CLT}} &= \int_{r_{\text{exc}}}^{\infty} Q\left(\frac{\sqrt{N}(P_{\text{th}} - I_{\text{tot,DI}}(r_{\text{dom}}) - \sigma_w^2)}{I_{\text{tot,DI}}(r_{\text{dom}}) + \sigma_w^2}\right) f_{R_{\text{dom}}}(r_{\text{dom}}) dr_{\text{dom}}, \\ \bar{P}_{\text{d,CLT}} &= \int_{r_{\text{exc}}}^{\infty} Q\left(\frac{\sqrt{N}(P_{\text{th}} - P_{\text{tar}} - I_{\text{tot,DI}}(r_{\text{dom}}) - \sigma_w^2)}{\sqrt{(P_{\text{tar}} + I_{\text{tot,DI}}(r_{\text{dom}}) + \sigma_w^2)^2 - P_{\text{tar}}^2}}\right) f_{R_{\text{dom}}}(r_{\text{dom}}) dr_{\text{dom}}.\end{aligned}\quad (29)$$

Proof. The proof is similar to Theorem 5, and follows from the complementary CDF of the Gaussian distribution in Corollary 4. ■

VI. NUMERICAL RESULTS AND DISCUSSION

In this section, we validate our theoretical results using Monte-Carlo simulations. We consider a typical radar operating at $f_c = 5$ GHz, located at the origin equipped with a $N_{\text{az}}^{(\text{rad})} \times N_{\text{el}}^{(\text{rad})}$ URA, mounted at a height of $h_{\text{rad}} = 20$ m. The radar is scanning a region above the horizon at $(\theta_{\text{rad}}, \phi_{\text{rad}}) = (60^\circ, -10^\circ)$. The BSs are distributed as a PPP, with varying intensities. Each massive MIMO BS is co-channel with the radar, and is equipped with a $N_{\text{az}}^{(\text{BS})} \times N_{\text{el}}^{(\text{BS})}$ URA deployed at a height of $h_{\text{BS}} = 50$ m. The circular exclusion zone around the radar has a *minimum radius* of $r_{\text{exc}}^{(\text{min})} = 5$ km. The boresight of each massive MIMO BS URA is aligned along the direction of the radar ($\theta_k = 0$ in the LCS). In each cell, the massive MIMO BS transmits a total power of $P_{\text{BS}} = 1$ W, equally allocated among co-scheduled UEs from $K = 4$ clusters with mutually disjoint angular support. To model the pathloss in the downlink and the BS to radar channels, we assume the 3GPP 3D Urban Macro (3D UMa) LoS pathloss model [41],

$$\begin{aligned}PL(d) &= P(h_{\text{BS}}, h_{\text{rad}}) + 20 \log_{10}(f_c) + 40 \log_{10}(d) \quad (\text{dB}), \\ P(h_{\text{BS}}, h_{\text{rad}}) &= 28 - 9 \log_{10}((h_{\text{BS}} - h_{\text{rad}})^2) \quad (\text{dB}),\end{aligned}$$

where f_c (GHz), and d (m).

A. Comparison of Worst-Case Average Interference under CBC and AAEC Models

Fig. 4 shows the average interference power derived in Section III under different cell models, as a function of exclusion zone radius for different BS intensities. We observe that the upper

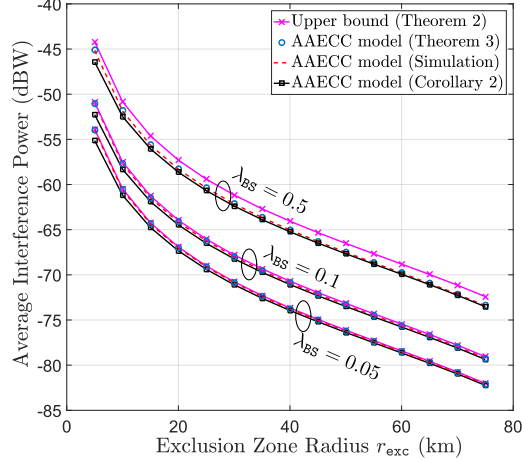


Fig. 4. Worst-case average interference power at the radar, as a function of exclusion zone radius, and different base station densities λ_{BS} (km^{-2}). $h_{\text{rad}} = 20$ m, $h_{\text{BS}} = 50$ m, $N_{\text{az}}^{(\text{BS})} = N_{\text{e1}}^{(\text{BS})} = 10$, $N_{\text{az}}^{(\text{rad})} = N_{\text{e1}}^{(\text{rad})} = 40$, $\theta_{\text{rad}} = 60^\circ$, $\phi_{\text{rad}} = -10^\circ$.

TABLE I
APPROXIMATE VALUES OF η_{ca}

$h_{\text{BS}}\sqrt{\pi\lambda_{\text{BS}}}$	0.0089	0.0198	0.028	0.044	0.0886	0.1253
η_{ca}	1.004	1.022	1.045	1.254	1.608	2.905

bound is remarkably tight, especially for low values of $\lambda_{\text{BS}} \leq 0.1$. For reference, we also plot the approximate average interference power from Corollary 1. It can be seen that its accuracy improves as r_{exc} increases, due to the accuracy of the underlying approximations regarding the elevation angle $\phi_{r,L}$. The approximately linear scaling of average interference power with λ_{BS} can also be observed, since the average interference power drops by ≈ 10 dB when λ_{BS} is decreased by an order of magnitude.

We also observe that the ratio of average interference powers η_{ca} is approximately constant, and is tabulated for the *elevation parameter* $h_{\text{BS}}\sqrt{\pi\lambda_{\text{BS}}}$ in Table I. For 3GPP UMa deployments with inter-site distance r_{ISD} , the typical $h_{\text{BS}}/r_{\text{ISD}} = 0.05$ [41]. The corresponding $h_{\text{BS}}\sqrt{\pi\lambda_{\text{BS}}} = 0.095$, for which $2 \text{ dB} < \eta_{\text{ca}} < 4.6 \text{ dB}$ (Table I). Thus the bound is remarkably tight, which makes it useful for worst-case analysis of practical radar-5G NR spectrum sharing deployments.

B. Distribution of Total Interference Power

Fig. 5 shows the distribution of total interference power for different exclusion zone radius, r_{exc} . Interestingly, we observe that the distribution concentrates in narrower intervals around the average interference power, with increasing r_{exc} . This is due to the fact that under the

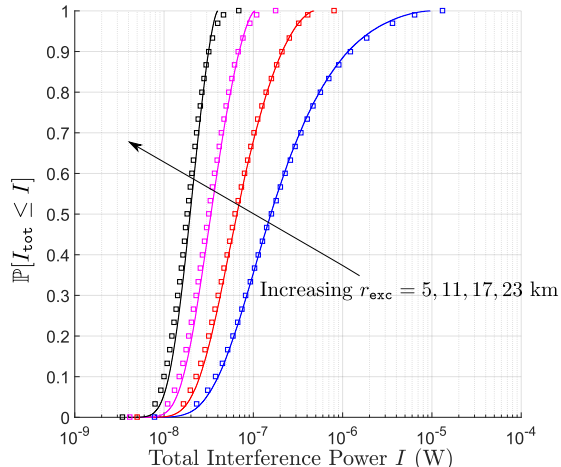


Fig. 5. Distribution of total interference power (I_{tot}) for $\lambda_{\text{BS}} = 0.01$ (km^{-2}), and different exclusion zone radii. Markers and solid lines represent the simulation and theoretical (Theorem 4) results respectively. $h_{\text{rad}} = 20$ m, $h_{\text{BS}} = 50$ m, $N_{\text{az}}^{(\text{BS})} = N_{\text{e1}}^{(\text{BS})} = 10$, $N_{\text{az}}^{(\text{rad})} = N_{\text{e1}}^{(\text{rad})} = 10$, $\theta_{\text{rad}} = 60^\circ$, $\phi_{\text{rad}} = -10^\circ$.

AAECC model, the average interference power scales as $r_{\text{exc}}^{-\alpha+2}$, while the corresponding standard deviation scales as $r_{\text{exc}}^{-\alpha+1}$, as shown in Corollary 2 (also refer [26]). Since the standard deviation decays faster with r_{exc} when compared to the average, the distribution of I_{tot} concentrates around the average power $\bar{I}_{\text{rad,a}}$, when r_{exc} increases.

Overall, the analytical expression in Theorem 4 obtained using the dominant interferer approximation matches well with the numerical results. However, we observe that there is a slight deviation in the upper tail of the CDF.

C. Radar Performance Metrics

Fig. 6 shows the radar performance metrics for different exclusion zone radii, in the case of a quasi-static target in the interference-limited regime. Fig. 6a and Fig. 6b show the spatial probability of detection and false alarm, as a function of the detection threshold (P_{th}). As expected, \bar{P}_{d} (\bar{P}_{fa}) monotonically increases (decreases) with r_{exc} respectively, for a fixed detection threshold. This is because expanding the exclusion zone improves the SINR of the received signal. We observe that there is a good match between the simulation results and the analytical results from Theorem 5. Furthermore, we also observe that the CLT approximation in Corollary 4 is remarkably accurate, even for a relatively small estimation window size of $N = 10$.

Fig. 6c shows the ROC curve for different r_{exc} values. We observe that the trends follow Figs. 6a-6b, and that the analytical and simulation results match. However, the inaccuracy due to the CLT approximation (Corollary 4) can be observed in the high \bar{P}_{d} -low \bar{P}_{fa} regime. This mismatch

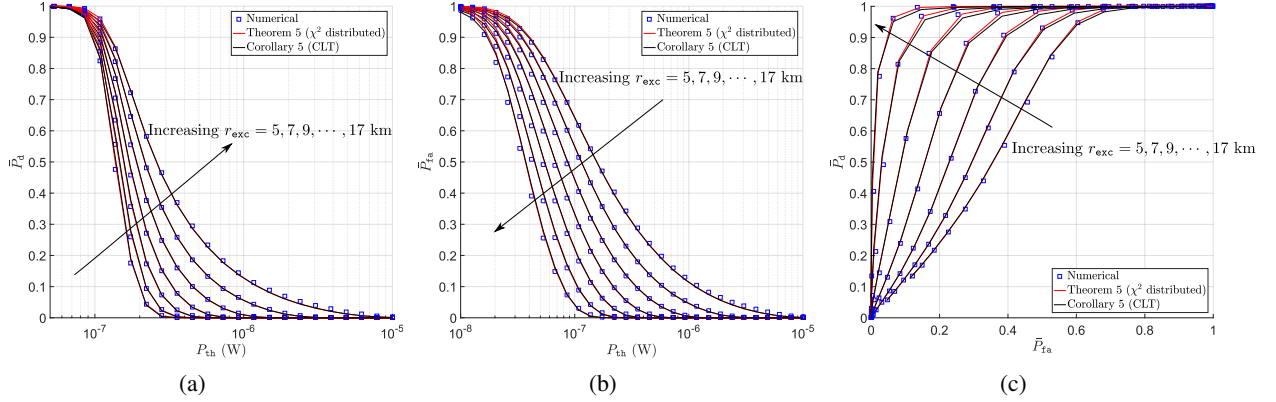


Fig. 6. Variation of (a) spatial probability of detection (\bar{P}_d), and (b) spatial probability of false alarm (\bar{P}_{fa}) as a function of the detection threshold (P_{th}) for different r_{exc} values. (c) ROC curve for different r_{exc} values. $\lambda_{BS} = 0.01 \text{ km}^{-2}$, $P_{tar} = 10^{-6} \text{ W}$, $\sigma_n^2 = 10^{-9} \text{ W}$, $h_{rad} = 20 \text{ m}$, $h_{BS} = 50 \text{ m}$, $N_{az}^{(BS)} = N_{e1}^{(BS)} = 10$, $N_{az}^{(rad)} = N_{e1}^{(rad)} = 10$, $\theta_{rad} = 60^\circ$, and $\phi_{rad} = -10^\circ$, $N = 10$.

is likely due to the difference in tail behavior of the Gaussian and χ^2 -distributions. Obtaining the ROC curves as a function of the operational parameters such as the r_{exc} , operating SNR etc., can be very helpful to determine the feasible set of deployment parameters in radar-cellular coexistence. Therefore, a key outcome of this work is a powerful mathematical tool to rapidly evaluate the radar system performance metrics in spectrum sharing scenarios with large massive MIMO cellular networks.

VII. CONCLUSION AND PROPOSED WORK

In this paper, we presented an analytical framework to evaluate radar performance metrics in underlay radar-massive MIMO cellular spectrum sharing scenarios, where both systems are equipped with 3D beamforming capabilities. We devised a novel construction based on bounding a PV cell by its circumcircle, to upper bound the worst-case average interference at the radar due to a co-channel massive MIMO downlink in near LoS channel conditions. We also proposed and analyzed the nominal average and variance of the interference power using a more tractable model, where each cell is replaced by a circular disk of area equal to the average area of a typical cell. We provided useful insights regarding the worst-case exclusion zone radius, scaling of interference power with BS density, and the approximate gap between the worst-case and nominal average interference power. We then derived the *equi-interference contour* under the nominal interference model, and used it to characterize the interference distribution, using the *dominant interference approximation*. Under a quasi-static target detection scenario based on

coherent integration across multiple radar pulses and threshold detection, we used the interference distribution to characterize the spatial probability of detection and false alarm.

Our analytical results were validated using Monte-Carlo simulations. We showed that the upper bound using the circumcircle-based model is remarkably tight for 3GPP deployment parameters [41]. More importantly, we demonstrated the usefulness of our proposed approach by applying it for evaluation of radar performance metrics, especially ROC curves. The analytical framework presented in this paper (a) enables network designers to systematically isolate and evaluate the impact of each deployment parameter (BS density, antenna height, transmit power, exclusion zone radius etc.) on the worst-case radar performance, and (b) complements industry-standard simulation methodologies, by establishing a baseline performance for each set of deployment parameters in practical spectrum sharing scenarios.

The emphasis on studying the impact of worst-case cellular interference obviated the need for modeling the aspects of scheduling in this work. Hence, a natural extension is to study a more realistic setup, by modeling the azimuth and elevation distributions of the scheduled user in the DIUC of each cell. In addition to the cellular downlink, characterizing the impact of cellular uplink interference on radar performance is also a relevant extension to this work. From a harmonious coexistence perspective, using this work to progress towards system-level optimization frameworks that seek to maximize the radar performance under cellular quality of service (QoS) constraints, and vice-versa, is an important research direction.

APPENDIX

A. Proof of Lemma 2

The steering vector of a $N_{\text{az}} \times N_{\text{el}}$ URA is $\mathbf{a}(\theta, \phi) = \mathbf{a}_{\text{az}}(\theta, \phi) \otimes \mathbf{a}_{\text{el}}(\phi)$, where \otimes is the Kronecker product. For $\frac{\lambda}{2}$ -spacing,

$$\begin{aligned}\mathbf{a}_{\text{az}}(\theta, \phi) &= [1 e^{-j\pi \sin \theta \cos \phi} \dots e^{-j\pi(N_{\text{az}}-1) \sin \theta \cos \phi}] \in \mathbb{C}^{N_{\text{az}} \times 1}, \\ \mathbf{a}_{\text{el}}(\phi) &= [1 e^{-j\pi \sin \phi} \dots e^{-j\pi(N_{\text{el}}-1) \sin \phi}] \in \mathbb{C}^{N_{\text{el}} \times 1}.\end{aligned}$$

Using the properties of the Kronecker product, expanding and simplifying, we get

$$G_{\text{BS}}(\theta, \phi, \theta_k, \phi_k) = \frac{\sin^2\left(\frac{\pi}{2}N_{\text{az}}(\sin \theta \cos \phi - \sin \theta_k \cos \phi_k)\right)}{N_{\text{az}} \sin^2\left(\frac{\pi}{2}(\sin \theta \cos \phi - \sin \theta_k \cos \phi_k)\right)} \cdot \frac{\sin^2\left(\frac{\pi}{2}N_{\text{el}}(\sin \phi - \sin \phi_k)\right)}{N_{\text{el}} \sin^2\left(\frac{\pi}{2}(\sin \phi - \sin \phi_k)\right)} \leq N_{\text{az}}N_{\text{el}}. \quad (30)$$

Since $\frac{\sin^2(Na)}{\sin^2 a} \leq N^2$ for $a \in \mathbb{R}$, the universal upper bound is obtained above, and is achieved when $a = 0$. To obtain a tighter bound $G_{\text{BS}}^{(\max)}$ defined in (6), we consider the following.

1) *Case 1:* If $\phi_m \leq \phi \leq \frac{\pi}{2}$, $G_{\text{BS}}(\theta, \phi, \theta_k, \phi_k)$ is maximized by $\phi_k = \phi$, $\theta_k = \theta$, yielding $G_{\text{BS}}^{(\max)}(\phi, \phi_m) = N_{\text{az}}N_{\text{e1}}$.

2) *Case 2:* By upper bounding the *azimuth beamforming gain* in (30), we get $G_{\text{BS}}(\theta, \phi, \theta_k, \phi_k) \leq N_{\text{az}} \frac{\sin^2\left(\frac{\pi}{2}N_{\text{e1}}(\sin\phi - \sin\phi_k)\right)}{N_{\text{e1}}\sin^2\left(\frac{\pi}{2}(\sin\phi - \sin\phi_k)\right)}$. The RHS monotonically decreases w.r.t. ϕ_k when $0 \leq \sin\phi_m \leq \frac{1+N_{\text{e1}}\sin\phi}{N_{\text{e1}}} \leq \frac{\pi}{2}$ and hence, the upper bound is $G_{\text{BS}}^{(\max)}(\phi, \phi_m) = \frac{N_{\text{az}}\sin^2\left(\frac{\pi}{2}N_{\text{e1}}(\sin\phi - \sin\phi_m)\right)}{N_{\text{e1}}\sin^2\left(\frac{\pi}{2}(\sin\phi - \sin\phi_m)\right)}$.

3) *Case 3:* If $\frac{1+N_{\text{e1}}\sin\phi}{N_{\text{e1}}} \leq \sin\phi_m$, the numerator of $G_{\text{BS}}^{(\max)}(\cdot)$ in case 2 can be upper bounded as $\sin^2(b) \leq 1 \forall b \in \mathbb{R}$, resulting in a monotonically decreasing function of ϕ_m . Hence, $G_{\text{BS}}^{(\max)}(\phi, \phi_m) = \frac{N_{\text{az}}}{N_{\text{e1}}\sin^2\left(\frac{\pi}{2}(\sin\phi - \sin\phi_m)\right)}$.

We note that the upper bound on the beamforming gain is independent of the azimuth angle, since the maximum azimuth beamforming gain can be upper bounded by N_{az} . Therefore for the sake of simplicity, we consider that the boresight of each BS is aligned along the direction of the radar, which corresponds to $\theta = 0^\circ$ as discussed in Assumption 2.

B. Proof of Theorem 2

Since the massive MIMO BS locations are modeled as an independent PPPs Φ_{BS} with intensity λ_{BS} , the worst-case average interference at the radar is given by Campbell's theorem using

$$\bar{I}_{\text{rad,c}} = \mathbb{E}\left[\mathbb{E}\left[\sum_{\mathbf{X} \in \Phi_{\text{int}}} \{I_{\text{rad}}^{(\text{w})}(\mathbf{X}, h_{\text{BS}}, h_{\text{rad}})|r_c\}\right] \middle| r_c\right] = \mathbb{E}\left[\int_{\mathbf{x} \in \Phi_{\text{int}}} \lambda_{\text{BS}} \{I_{\text{rad}}^{(\text{w})}(\mathbf{x}, h_{\text{BS}}, h_{\text{rad}})|r_c\} d\mathbf{x} \middle| r_c\right],$$

where $\mathbf{x} = [r \cos \theta_{r,L} \ r \sin \theta_{r,L}]$, $\Phi_{\text{int}} = \Phi_{\text{BS}} \setminus \{(x, y) | (x^2 + y^2) \leq r_{\text{exc}}^2\}$, and r_c is the cell radius that determines $G_{\text{BS}}^{(\max)}(\phi, \phi_m)$ in equation (6). Substituting (4) above, noting that $\phi_{r,L}(r) = -\phi_{t,L}(r) = \tan^{-1}\left(\frac{h_{\text{rad}} - h_{\text{BS}}}{r}\right)$, and converting to polar coordinates we get

$$\bar{I}_{\text{rad,c}} = \mathbb{E}\left[\int_{r_{\text{exc}}}^{\infty} \int_{-\frac{\pi}{2}}^{\frac{\pi}{2}} \lambda_{\text{BS}} \beta(d) G_{\text{rad}}(\theta_{\text{rad}}, \phi_{\text{rad}}, \theta_{r,L}, \phi_{r,L}(r)) G_{\text{BS}}^{(\max)}(\phi_{t,L}(r), \phi_m(r_c)) \frac{P_{\text{BS}}}{K} r dr d\theta_{r,L} \middle| r_c\right],$$

where $d = \sqrt{r^2 + (h_{\text{BS}} - h_{\text{rad}})^2}$, and $\beta(d) = PL(r_0)d^{-\alpha}$ is the pathloss model. Using these and integrating over $r_c \sim f_{R_c}(r_c)$, we get the desired result.

C. Proof of Lemma 3

Since r_{exc} is much larger than the antenna heights, we have $\phi(r) \rightarrow 0$ for $r \geq r_{\text{exc}}$ in equation (13) and (14). Using this, the radar beamforming gain can be upper bounded similar to (30) as

$$G_{\text{rad}}(\theta_{\text{rad}}, \phi_{\text{rad}}, \theta, 0) = \frac{\sin^2\left(\frac{\pi}{2}N_{\text{az}}^{(\text{rad})}(\sin\theta_{\text{rad}}\cos\phi_{\text{rad}} - \sin\theta)\right) \sin^2\left(\frac{\pi}{2}N_{\text{e1}}^{(\text{rad})}\sin\phi_{\text{rad}}\right)}{N_{\text{az}}^{(\text{rad})}N_{\text{e1}}^{(\text{rad})}\sin^2\left(\frac{\pi}{2}(\sin\theta_{\text{rad}}\cos\phi_{\text{rad}} - \sin\theta)\right) \sin^2\left(\frac{\pi}{2}\sin\phi_{\text{rad}}\right)} \leq \frac{N_{\text{az}}^{(\text{rad})}\sin^2\left(\frac{\pi}{2}N_{\text{e1}}^{(\text{rad})}\sin\phi_{\text{rad}}\right)}{N_{\text{e1}}^{(\text{rad})}\sin^2\left(\frac{\pi}{2}\sin\phi_{\text{rad}}\right)}.$$

We note that the maximum azimuth beamforming gain of N_{az} is always achieved at $\theta_{\text{max}} = \sin^{-1}(\sin\theta_{\text{rad}}\cos\phi_{\text{rad}})$. Therefore, the maximum radar beamforming gain is only a function of

ϕ_{rad} . For similar reasons, when $\phi(r) \rightarrow 0$, $G_{BS}^{(\max)}(\cdot)$ is only a function of the minimum elevation angle, which in turn is a function of $h_{BS}\sqrt{\lambda_{BS}}$.

Defining I_{dom} to be the interference power due to the BS at $(r_{\text{dom}}, \theta_{\text{max}})$, given by $I_{\text{dom}} = \frac{P_{BSPL}(r_0)G_{BS}^{(\max)}(0, \phi_m(1/\sqrt{\pi\lambda_{BS}}))}{Kr_{\text{dom}}^\alpha} \cdot \frac{N_{\text{az}}^{(\text{rad})} \sin^2\left(\frac{\pi}{2}N_{\text{e1}}^{(\text{rad})} \sin \phi_{\text{rad}}\right)}{N_{\text{e1}}^{(\text{rad})} \sin^2\left(\frac{\pi}{2} \sin \phi_{\text{rad}}\right)}$, $r_{\text{dom}} \geq r_{\text{exc}}$. Substituting this into equation (14) and simplifying, we get the analytical expression of $\mathcal{C}(I_{\text{dom}})$.

D. Proof of Lemma 4

Let $\mathcal{A}(r_{\text{dom}})$ denote the region outside the exclusion zone enclosed by $\mathcal{C}(r_{\text{dom}})$, and $A(r_{\text{dom}})$ denote the corresponding area. Using equation (13), this region can be written as

$$\mathcal{A}(r_{\text{dom}}) = \left\{ (r, \theta) \mid r_{\text{exc}} \leq r \leq \max\left(r_{\text{exc}}, r_{\text{dom}} \left[\frac{\sin\left(\frac{\pi}{2}N_{\text{az}}^{(\text{rad})}(\sin \theta_{\text{rad}} \cos \phi_{\text{rad}} - \sin \theta)\right)}{N_{\text{az}}^{(\text{rad})} \sin^2\left(\frac{\pi}{2}(\sin \theta_{\text{rad}} \cos \phi_{\text{rad}} - \sin \theta)\right)} \right]^{\frac{2}{\alpha}}\right), \right. \\ \left. -\frac{\pi}{2} \leq \theta \leq \frac{\pi}{2} \right\}. \quad (31)$$

Defining $\tilde{r}_{\text{dom}}(\theta) \triangleq r_{\text{dom}} \left[\frac{\sin\left(\frac{\pi}{2}N_{\text{az}}^{(\text{rad})}(\sin \theta_{\text{rad}} \cos \phi_{\text{rad}} - \sin \theta)\right)}{N_{\text{az}}^{(\text{rad})} \sin^2\left(\frac{\pi}{2}(\sin \theta_{\text{rad}} \cos \phi_{\text{rad}} - \sin \theta)\right)} \right]^{\frac{2}{\alpha}}$ and using equation (31), the area $A(r_{\text{dom}})$ is given by

$$A(r_{\text{dom}}) = \int_{-\frac{\pi}{2}}^{\frac{\pi}{2}} \int_{r_{\text{exc}}}^{\max(r_{\text{exc}}, \tilde{r}_{\text{dom}}(\theta))} r dr d\theta = \frac{1}{2} \int_{-\frac{\pi}{2}}^{\frac{\pi}{2}} \max(r_{\text{exc}}^2, \tilde{r}_{\text{dom}}^2(\theta)) d\theta - \frac{\pi r_{\text{exc}}^2}{2}. \quad (32)$$

Expanding and simplifying, we get the desired result.

E. Proof of Lemma 5

The distribution of r_{dom} is given by $F_{R_{\text{dom}}}(r_{\text{dom}}) = \mathbb{P}[R_{\text{dom}} \leq r_{\text{dom}}]$. Since the area outside the exclusion zone enclosed by the contour is $A(r_{\text{dom}})$, the CDF is the void probability given by

$$F_{R_{\text{dom}}}(r_{\text{dom}}) = 1 - \exp(-\lambda_{BS}A(r_{\text{dom}})), \text{ for } r_{\text{dom}} \geq r_{\text{exc}}. \quad (33)$$

Substitution equation (16) in the above, we get the desired CDF. Further, differentiating equation (33), the density of r_{dom} can be written as

$$f_{R_{\text{dom}}}(r_{\text{dom}}) = \frac{dA(r_{\text{dom}})}{dr_{\text{dom}}} \cdot \lambda_{BS}e^{-\lambda_{BS}A(r_{\text{dom}})}, \text{ for } r_{\text{dom}} \geq r_{\text{exc}}. \quad (34)$$

Due to the presence of the $\max(\cdot)$ term in equation (16), it can be shown that $A(r_{\text{dom}})$ depends on r_{dom} only in certain ranges of θ , which can also be observed in Fig. 3b. Hence, we get

$$\frac{d[\max(r_{\text{exc}}^2, \tilde{r}_{\text{dom}}^2(\theta))]}{dr_{\text{dom}}} = \begin{cases} 2r_{\text{dom}} \left[\frac{\sin^2\left(\frac{\pi}{2}N_{\text{az}}(\sin \theta_{\text{rad}} \cos \phi_{\text{rad}} - \sin \theta)\right)}{N_{\text{az}}^2 \sin^2\left(\frac{\pi}{2}(\sin \theta_{\text{rad}} \cos \phi_{\text{rad}} - \sin \theta)\right)} \right]^{2/\alpha} & \text{if } \tilde{r}_{\text{dom}}(\theta) \geq r_{\text{exc}} \\ 0 & \text{otherwise} \end{cases}, \quad (35)$$

Substituting this into (34) and representing it in terms of the indicator function, we obtain the desired result.

F. Proof of Theorem 4

The dominant interference power is given by $I_{\text{dom}} = \kappa r_{\text{dom}}^{-\alpha}$. Next, we compute the average interference power due to the rest of the network, conditioned on I_{dom} , i.e. $\mathbb{E}[I_{\text{rest}}|I_{\text{dom}}]$. Due to the bijection between r_{dom} and I_{dom} in the AAEC model, we have $\mathbb{E}[I_{\text{rest}}|I_{\text{dom}}] = \mathbb{E}[I_{\text{rest}}|r_{\text{dom}}]$. Hence, we can compute the conditional average interference power using

$$\begin{aligned} \mathbb{E}[I_{\text{rest}}|I_{\text{dom}}] &= \frac{P_{BS}\lambda_{BS}G_{BS}(0,\phi_m(1/\sqrt{\pi\lambda_{BS}}))PL(r_0)}{K} \int_{-\frac{\pi}{2}}^{\frac{\pi}{2}} \int_{\max(r_{\text{exc}}, \tilde{r}_{\text{dom}}(\theta))}^{\infty} G_{\text{rad}}(0, \phi_{\text{rad}}, \theta, 0) r^{-\alpha+1} dr d\theta \\ &\stackrel{(a)}{=} \frac{\kappa}{\alpha-2} \int_{-\frac{\pi}{2}}^{\frac{\pi}{2}} [\max(r_{\text{exc}}, \tilde{r}_{\text{dom}}(\theta))]^{-\alpha+2} \frac{G_{\text{rad}}(\theta_{\text{rad}}, \phi_{\text{rad}}, \theta, 0)}{G_{\text{rad}}(0, \phi_{\text{rad}}, 0, 0)} d\theta. \end{aligned} \quad (36)$$

The equality in (a) is obtained by defining $\kappa \triangleq \frac{P_{BS}\lambda_{BS}G_{\text{rad}}(0,\phi_{\text{rad}},0,0)G_{BS}(0,\phi_m(1/\sqrt{\pi\lambda_{BS}}))PL(r_0)}{K}$, and evaluating the inner integral. Using Lemma 3 and equation (36) in equation (12) and simplifying, we get the desired result.

G. Proof of Theorem 5

We note that under hypothesis \mathcal{H}_i , the received power is $P_{\text{rad},i}$ for $i = \{0, 1\}$. In addition, by definition we have $\mathbb{P}[P_{\text{rad},i} > P_{\text{th}}|I_{\text{tot}}] = 1 - F_{P_{\text{rad},i}}(P_{\text{th}}|I_{\text{tot}})$. Therefore, using Lemma 7, we can write equation (27) as

$$\begin{aligned} \bar{P}_d &= 1 - \int_0^{\infty} Q_N\left(\sqrt{\frac{2NP_{\text{tar}}}{I_{\text{tot}}+\sigma_n^2}}, \sqrt{\frac{2NP_{\text{th}}}{I_{\text{tot}}+\sigma_n^2}}\right) f_{I_{\text{tot}}}(x) dx, \\ \bar{P}_{\text{fa}} &= 1 - \int_0^{\infty} \frac{1}{(N-1)!} \gamma_l\left(N, \frac{NP_{\text{th}}}{I_{\text{tot}}+\sigma_n^2}\right) f_{I_{\text{tot}}}(x) dx. \end{aligned} \quad (37)$$

The first approximation is obtained by replacing I_{tot} by $I_{\text{tot,DI}}$ using Theorem 4, and changing the upper limit to $I_{\text{exc}} + \bar{I}_{\text{rad,a}}$ (Remark 2). Using the bijection between r_{dom} and $I_{\text{tot,DI}}$ (Corollary 3), the final result is obtained by substituting $I_{\text{tot,DI}}$ by r_{dom} , and applying the chain rule.

REFERENCES

- [1] R. M. Rao, H. S. Dhillon, V. Marojevic, and J. H. Reed, "Analysis of Worst-Case Interference in Underlay Radar-Massive MIMO Spectrum Sharing Scenarios," in *2019 IEEE Global Communications Conference (GLOBECOM)*, 2019, pp. 1–6.
- [2] S. M. Dudley, W. C. Headley, M. Lichtman, E. Y. Imana, X. Ma, M. Abdelbar, A. Padaki, A. Ullah, M. M. Sohul, T. Yang, and J. H. Reed, "Practical Issues for Spectrum Management With Cognitive Radios," *Proceedings of the IEEE*, vol. 102, no. 3, pp. 242–264, 2014.
- [3] T. L. Marzetta, "Noncooperative Cellular Wireless with Unlimited Numbers of Base Station Antennas," *IEEE Transactions on Wireless Communications*, vol. 9, no. 11, pp. 3590–3600, November 2010.
- [4] A. Adhikary, J. Nam, J. Ahn, and G. Caire, "Joint Spatial Division and Multiplexing-The Large-Scale Array Regime," *IEEE Transactions on Information Theory*, vol. 59, no. 10, pp. 6441–6463, Oct 2013.

- [5] X. Gao, O. Edfors, F. Rusek, and F. Tufvesson, "Massive MIMO Performance Evaluation Based on Measured Propagation Data," *IEEE Transactions on Wireless Communications*, vol. 14, no. 7, pp. 3899–3911, July 2015.
- [6] G. Xu, Y. Li, J. Yuan, R. Monroe, S. Rajagopal, S. Ramakrishna, Y. H. Nam, J. Seol, J. Kim, M. M. U. Gul, A. Aziz, and J. Zhang, "Full Dimension MIMO (FD-MIMO): Demonstrating Commercial Feasibility," *IEEE Journal on Selected Areas in Communications*, vol. 35, no. 8, pp. 1876–1886, Aug 2017.
- [7] H. Ji, Y. Kim, J. Lee, E. Onggosanusi, Y. Nam, J. Zhang, B. Lee, and B. Shim, "Overview of Full-Dimension MIMO in LTE-Advanced Pro," *IEEE Communications Magazine*, vol. 55, no. 2, pp. 176–184, February 2017.
- [8] FCC, "Amendment of the Commission's Rules with Regard to Commercial Operations in the 3550-3650 MHz Band," *Federal Communications Commission, Report and Order and Second Further Notice of Proposed Rulemaking*, April 2015.
- [9] —, "Revision of Part 15 of the Commission's Rules to Permit Unlicensed National Information Infrastructure (U-NII) Devices in the 5 GHz Band," *Federal Communications Commission, First Report and Order*, April 2014.
- [10] H. Kwon, J. Jeon, A. Bhorkar, Q. Ye, H. Harada, Y. Jiang, L. Liu, S. Nagata, B. L. Ng, T. Novlan, J. Oh, and W. Yi, "Licensed-Assisted Access to Unlicensed Spectrum in LTE Release 13," *IEEE Communications Magazine*, vol. 55, no. 2, pp. 201–207, February 2017.
- [11] A. Ghosh, A. Maeder, M. Baker, and D. Chandramouli, "5G Evolution: A View on 5G Cellular Technology Beyond 3GPP Release 15," *IEEE Access*, vol. 7, pp. 127 639–127 651, 2019.
- [12] F. Liu, C. Masouros, A. Li, and T. Ratnarajah, "Robust MIMO Beamforming for Cellular and Radar Coexistence," *IEEE Wireless Communications Letters*, vol. 6, no. 3, pp. 374–377, June 2017.
- [13] S. Biswas, K. Singh, O. Taghizadeh, and T. Ratnarajah, "Coexistence of MIMO Radar and FD MIMO Cellular Systems With QoS Considerations," *IEEE Transactions on Wireless Communications*, vol. 17, no. 11, pp. 7281–7294, Nov 2018.
- [14] B. Li, A. P. Petropulu, and W. Trappe, "Optimum Co-Design for Spectrum Sharing between Matrix Completion Based MIMO Radars and a MIMO Communication System," *IEEE Transactions on Signal Processing*, vol. 64, no. 17, pp. 4562–4575, Sep. 2016.
- [15] J. A. Mahal, A. Khawar, A. Abdelhadi, and T. C. Clancy, "Spectral Coexistence of MIMO Radar and MIMO Cellular System," *IEEE Transactions on Aerospace and Electronic Systems*, vol. 53, no. 2, pp. 655–668, April 2017.
- [16] M. Bica, K. Huang, V. Koivunen, and U. Mitra, "Mutual Information based Radar Waveform Design for Joint Radar and Cellular Communication Systems," in *2016 IEEE International Conference on Acoustics, Speech and Signal Processing (ICASSP)*, March 2016, pp. 3671–3675.
- [17] B. Tang and J. Li, "Spectrally Constrained MIMO Radar Waveform Design Based on Mutual Information," *IEEE Transactions on Signal Processing*, vol. 67, no. 3, pp. 821–834, Feb 2019.
- [18] S. Kim, J. Choi, and C. Dietrich, "PSUN: An OFDM-Pulsed Radar Coexistence Technique with Application to 3.5 GHz LTE," *Mobile Information Systems*, vol. 2016, 2016.
- [19] M. Carrick, J. H. Reed, and C. M. Spooner, "Mitigating Linear-Frequency-Modulated Pulsed Radar Interference to OFDM," *IEEE Transactions on Aerospace and Electronic Systems*, vol. 55, no. 3, pp. 1146–1159, June 2019.
- [20] R. Saruthirathanaworakun, J. M. Peha, and L. M. Correia, "Opportunistic Sharing Between Rotating Radar and Cellular," *IEEE Journal on Selected Areas in Communications*, vol. 30, no. 10, pp. 1900–1910, November 2012.
- [21] Z. Khan, J. J. Lehtomaki, R. Vuoltoniemi, E. Hossain, and L. A. Dasilva, "On Opportunistic Spectrum Access in Radar Bands: Lessons Learned from Measurement of Weather Radar Signals," *IEEE Wireless Communications*, vol. 23, no. 3, pp. 40–48, June 2016.
- [22] F. Liu, A. Garcia-Rodriguez, C. Masouros, and G. Geraci, "Interfering Channel Estimation in Radar-Cellular Coexistence: How Much Information Do We Need?" *IEEE Trans. Wireless Commun.*, vol. 18, no. 9, pp. 4238–4253, Sep. 2019.
- [23] Y. Li, F. Baccelli, J. G. Andrews, T. D. Novlan, and J. C. Zhang, "Modeling and Analyzing the Coexistence of Wi-Fi and LTE in Unlicensed Spectrum," *IEEE Transactions on Wireless Communications*, vol. 15, no. 9, pp. 6310–6326, Sep. 2016.

- [24] H. Hu, Y. Gao, J. Zhang, X. Chu, Q. Chen, and J. Zhang, "Density Analysis of LTE-LAA Networks Coexisting With WiFi Sharing Multiple Unlicensed Channels," *IEEE Access*, vol. 7, pp. 148 004–148 018, 2019.
- [25] P. Parida, H. S. Dhillon, and P. Nuggehalli, "Stochastic Geometry-Based Modeling and Analysis of Citizens Broadband Radio Service System," *IEEE Access*, vol. 5, pp. 7326–7349, 2017.
- [26] F. Hesar and S. Roy, "Spectrum Sharing between a Surveillance Radar and Secondary Wi-Fi Networks," *IEEE Transactions on Aerospace and Electronic Systems*, vol. 52, no. 3, pp. 1434–1448, June 2016.
- [27] S. Kim and C. Dietrich, "Coexistence of Outdoor Wi-Fi and Radar at 3.5 GHz," *IEEE Wireless Communications Letters*, vol. 6, no. 4, pp. 522–525, Aug 2017.
- [28] H. Chen, L. Liu, H. S. Dhillon, and Y. Yi, "QoS-Aware D2D Cellular Networks With Spatial Spectrum Sensing: A Stochastic Geometry View," *IEEE Transactions on Communications*, vol. 67, no. 5, pp. 3651–3664, 2019.
- [29] H. Chen, L. Liu, T. Novlan, J. D. Matyjias, B. L. Ng, and J. Zhang, "Spatial Spectrum Sensing-Based Device-to-Device Cellular Networks," *IEEE Transactions on Wireless Communications*, vol. 15, no. 11, pp. 7299–7313, 2016.
- [30] B. Shang, L. Liu, R. M. Rao, V. Marojevic, and J. H. Reed, "3D Spectrum Sharing for Hybrid D2D and UAV Networks," *IEEE Transactions on Communications*, vol. 68, no. 9, pp. 1–1, 2020.
- [31] T. Bai and R. W. Heath, "Coverage and Rate Analysis for Millimeter-Wave Cellular Networks," *IEEE Transactions on Wireless Communications*, vol. 14, no. 2, pp. 1100–1114, 2015.
- [32] M. Rebato, J. Park, P. Popovski, E. De Carvalho, and M. Zorzi, "Stochastic Geometric Coverage Analysis in mmWave Cellular Networks With Realistic Channel and Antenna Radiation Models," *IEEE Transactions on Communications*, vol. 67, no. 5, pp. 3736–3752, 2019.
- [33] S. Kim, E. Visotsky, P. Moorut, K. Bechta, A. Ghosh, and C. Dietrich, "Coexistence of 5G With the Incumbents in the 28 and 70 GHz Bands," *IEEE Journal on Selected Areas in Communications*, vol. 35, no. 6, pp. 1254–1268, June 2017.
- [34] M. Baianifar, S. Khavari, S. M. Razavizadeh, and T. Svensson, "Impact of User Height on the Coverage of 3D Beamforming-enabled Massive MIMO Systems," in *2017 IEEE 28th Annual International Symposium on Personal, Indoor, and Mobile Radio Communications (PIMRC)*, Oct 2017, pp. 1–5.
- [35] J. Yang, M. Ding, G. Mao, Z. Lin, D. Zhang, and T. H. Luan, "Optimal Base Station Antenna Downtilt in Downlink Cellular Networks," *IEEE Transactions on Wireless Communications*, pp. 1–1, 2019.
- [36] P. Calka, "The Distributions of the Smallest Disks Containing the Poisson-Voronoi Typical Cell and the Crofton Cell in the Plane," *Advances in Applied Probability*, vol. 34, no. 4, pp. 702–717, 2002.
- [37] V. V. Chetlur and H. S. Dhillon, "Downlink Coverage Analysis for a Finite 3-D Wireless Network of Unmanned Aerial Vehicles," *IEEE Transactions on Communications*, vol. 65, no. 10, pp. 4543–4558, 2017.
- [38] J. Schloemann, H. S. Dhillon, and R. M. Buehrer, "Toward a Tractable Analysis of Localization Fundamentals in Cellular Networks," *IEEE Transactions on Wireless Communications*, vol. 15, no. 3, pp. 1768–1782, 2016.
- [39] R. W. Heath, M. Kountouris, and T. Bai, "Modeling Heterogeneous Network Interference Using Poisson Point Processes," *IEEE Transactions on Signal Processing*, vol. 61, no. 16, pp. 4114–4126, 2013.
- [40] X. Kang, Y. Liang, H. K. Garg, and L. Zhang, "Sensing-Based Spectrum Sharing in Cognitive Radio Networks," *IEEE Transactions on Vehicular Technology*, vol. 58, no. 8, pp. 4649–4654, 2009.
- [41] ETSI, "5G; Study on channel model for frequencies from 0.5 to 100 GHz (3GPP TR 38.901 version 14.0.0 Release 14)," *3GPP*, May 2017.
- [42] J. G. Andrews, A. K. Gupta, and H. S. Dhillon, "A Primer on Cellular Network Analysis using Stochastic Geometry," *arXiv preprint arXiv:1604.03183*, 2016.
- [43] M. Haenggi, "On Distances in Uniformly Random Networks," *IEEE Transactions on Information Theory*, vol. 51, no. 10, pp. 3584–3586, 2005.